Identified charged-hadron production in p + Al, ^{3}He +Au, and Cu + Au collisions at $\sqrt{s_{NN}} = 200$ GeV and in U + U collisions at $\sqrt{s_{NN}} = 193$ GeV

N. J. Abdulameer,[15] U. Acharya,[20] A. Adare,[12] C. Aidala,[39,45] N. N. Ajitanand,[66,*] Y. Akiba,[61,62,†] R. Akimoto,[11] J. Alexander,[66] M. Alfred,[23] V. Andrieux,[45] K. Aoki,[32,61] N. Apadula,[28,67] H. Asano,[35,61] E. T. Atomssa,[67] T. C. Awes,[56] B. Azmoun,[7] V. Babintsev,[24] M. Bai,[6] X. Bai,[10] N. S. Bandara,[43] B. Bannier,[67] K. N. Barish,[8] S. Bathe,[5,62] V. Baublis,[59] C. Baumann,[7] S. Baumgart,[61] A. Bazilevsky,[7] M. Beaumier,[8] S. Beckman,[12] R. Belmont,[12,45,54,73] A. Berdnikov,[64] Y. Berdnikov,[64] L. Bichon,[73] D. Black,[8] B. Blankenship,[73] D. S. Blau,[34,51] J. S. Bok,[53] V. Borisov,[64] K. Boyle,[62] M. L. Brooks,[39] J. Bryslawskyj,[5,8] H. Buesching,[7] V. Bumazhnov,[24] S. Butsyk,[52] S. Campbell,[13,28] V. Canoa Roman,[67] R. Cervantes,[67] C.-H. Chen,[62] D. Chen,[67] M. Chiu,[7] C. Y. Chi,[13] I. J. Choi,[25] J. B. Choi,[30,*] S. Choi,[65] P. Christiansen,[40] T. Chujo,[72] V. Cianciolo,[56] Z. Citron,[74] B. A. Cole,[13] M. Connors,[20,62] R. Corliss,[67] Y. Corrales Morales,[39] N. Cronin,[47,67] N. Crossette,[47] M. Csanád,[16] T. Csörgő,[44,75] L. D'Orazio,[42] T. W. Danley,[55] A. Datta,[52] M. S. Daugherity,[1] G. David,[7,67] C. T. Dean,[39] K. DeBlasio,[52] K. Dehmelt,[67] A. Denisov,[24] A. Deshpande,[62,67] E. J. Desmond,[7] L. Ding,[28] A. Dion,[67] P. B. Diss,[42] D. Dixit,[67] V. Doomra,[67] J. H. Do,[76] O. Drapier,[36] A. Drees,[67] K. A. Drees,[6] J. M. Durham,[39] A. Durum,[24] H. En'yo,[61,62] T. Engelmore,[13] A. Enokizono,[61,63] R. Esha,[67] K. O. Eyser,[7] B. Fadem,[47] W. Fan,[67] N. Feege,[67] D. E. Fields,[52] M. Finger, Jr.,[9] M. Finger,[9] D. Firak,[15,67] D. Fitzgerald,[45] F. Fleuret,[36] S. L. Fokin,[34] J. E. Frantz,[55] A. Franz,[7] A. D. Frawley,[19] Y. Fukao,[32] Y. Fukuda,[72] T. Fusayasu,[49] K. Gainey,[1] P. Gallus,[14] C. Gal,[67] P. Garg,[3,67] A. Garishvili,[69] I. Garishvili,[38] H. Ge,[67] M. Giles,[67] F. Giordano,[25] A. Glenn,[38] X. Gong,[66] M. Gonin,[36] Y. Goto,[61,62] R. Granier de Cassagnac,[36] N. Grau,[2] S. V. Greene,[73] M. Grosse Perdekamp,[25] Y. Gu,[66] T. Gunji,[11] T. Guo,[67] H. Guragain,[20] T. Hachiya,[50,61,62] J. S. Haggerty,[7] K. I. Hahn,[17] H. Hamagaki,[11] H. F. Hamilton,[1] J. Hanks,[67] S. Y. Han,[17,33] M. Harvey,[70] S. Hasegawa,[29] T. O. S. Haseler,[20] K. Hashimoto,[61,63] R. Hayano,[11] T. K. Hemmick,[67] T. Hester,[8] X. He,[20] J. C. Hill,[28] K. Hill,[12] A. Hodges,[20,25] R. S. Hollis,[8] K. Homma,[22] B. Hong,[33] T. Hoshino,[22] N. Hotvedt,[28] J. Huang,[7,39] T. Ichihara,[61,62] Y. Ikeda,[61] K. Imai,[29] Y. Imazu,[61] M. Inaba,[72] A. Iordanova,[8] D. Isenhower,[1] A. Isinhue,[47] D. Ivanishchev,[59] B. V. Jacak,[67] S. J. Jeon,[48] M. Jezghani,[20] X. Jiang,[39] Z. Ji,[67] B. M. Johnson,[7,20] K. S. Joo,[48] D. Jouan,[57] D. S. Jumper,[25] J. Kamin,[67] S. Kanda,[11,32] B. H. Kang,[21] J. H. Kang,[76] J. S. Kang,[21] D. Kapukchyan,[8] J. Kapustinsky,[39] S. Karthas,[67] D. Kawall,[43] A. V. Kazantsev,[34] J. A. Key,[52] V. Khachatryan,[67] P. K. Khandai,[3] A. Khanzadeev,[59] A. Khatiwada,[39] K. M. Kijima,[22] B. Kimelman,[47] C. Kim,[8,33] D. J. Kim,[31] E.-J. Kim,[30] G. W. Kim,[17] M. Kim,[65] T. Kim,[17] Y.-J. Kim,[25] Y. K. Kim,[21] D. Kincses,[16] A. Kingan,[67] E. Kistenev,[7] R. Kitamura,[11] J. Klatsky,[19] D. Kleinjan,[8] P. Kline,[67] T. Koblesky,[12] M. Kofarago,[16,75] B. Komkov,[59] J. Koster,[62] D. Kotchetkov,[55] D. Kotov,[59,64] L. Kovacs,[16] F. Krizek,[31] S. Kudo,[72] B. Kurgyis,[16,67] K. Kurita,[63] M. Kurosawa,[61,62] Y. Kwon,[76] Y. S. Lai,[13] J. G. Lajoie,[28] D. Larionova,[64] A. Lebedev,[28] D. M. Lee,[39] G. H. Lee,[30] J. Lee,[17,68] K. B. Lee,[39] K. S. Lee,[33] S. Lee,[76] S. H. Lee,[28,45,67] M. J. Leitch,[39] M. Leitgab,[25] Y. H. Leung,[67] B. Lewis,[67] N. A. Lewis,[45] S. H. Lim,[39,60,76] M. X. Liu,[39] X. Li,[10] X. Li,[39] V.-R. Loggins,[25] S. Lökös,[16] D. A. Loomis,[45] K. Lovasz,[15] D. Lynch,[7] C. F. Maguire,[73] T. Majoros,[15] Y. I. Makdisi,[6] M. Makek,[74,77] A. Manion,[67] V. I. Manko,[34] E. Mannel,[7] M. McCumber,[12,39] P. L. McGaughey,[39] D. McGlinchey,[12,19,39] C. McKinney,[25] A. Meles,[53] M. Mendoza,[8] B. Meredith,[25] Y. Miake,[72] T. Mibe,[32] A. C. Mignerey,[42] A. Milov,[74] D. K. Mishra,[4] J. T. Mitchell,[7] Iu. Mitrankov,[64,67] M. Mitrankova,[64,67] G. Mitsuka,[32,62] S. Miyasaka,[61,71] S. Mizuno,[61,72] A. K. Mohanty,[4] S. Mohapatra,[66] M. M. Mondal,[67] P. Montuenga,[25] T. Moon,[33,76] D. P. Morrison,[7] M. Moskowitz,[47] T. V. Moukhanova,[34] A. Muhammad,[46] B. Mulilo,[33,61,78] T. Murakami,[35,61] J. Murata,[61,63] A. Mwai,[66] T. Nagae,[35] K. Nagai,[71] S. Nagamiya,[32,61] K. Nagashima,[22] T. Nagashima,[63] J. L. Nagle,[12] M. I. Nagy,[16] I. Nakagawa,[61,62] H. Nakagomi,[61,72] Y. Nakamiya,[22] K. R. Nakamura,[35,61] T. Nakamura,[61] K. Nakano,[61,71] C. Nattrass,[69] S. Nelson,[18] P. K. Netrakanti,[4] M. Nihashi,[22,61] T. Niida,[72] S. Nishimura,[11] R. Nouicer,[7,62] T. Novák,[44,75] N. Novitzky,[31,67,72] G. Nukazuka,[61,62] A. S. Nyanin,[34] E. O'Brien,[7] C. A. Ogilvie,[28] J. Oh,[60] H. Oide,[11] K. Okada,[62] J. D. Orjuela Koop,[12] M. Orosz,[15] J. D. Osborn,[45,56] A. Oskarsson,[40] G. J. Ottino,[52] K. Ozawa,[32,72] R. Pak,[7] V. Pantuev,[26] V. Papavassiliou,[53] I. H. Park,[17,68] J. S. Park,[65] S. Park,[46,61,65,67] S. K. Park,[33] L. Patel,[20] M. Patel,[28] S. F. Pate,[53] J.-C. Peng,[25] W. Peng,[73] D. V. Perepelitsa,[7,12,13] G. D. N. Perera,[53] D.Yu. Peressounko,[34] C. E. PerezLara,[67] J. Perry,[28] R. Petti,[7,67] M. Phipps,[7,25] C. Pinkenburg,[7] R. Pinson,[1] R. P. Pisani,[7] M. Potekhin,[7] A. Pun,[55] M. L. Purschke,[7] H. Qu,[1] P. V. Radzevich,[64] J. Rak,[31] N. Ramasubramanian,[67] B. J. Ramson,[45] I. Ravinovich,[74] K. F. Read,[56,69] D. Reynolds,[66] V. Riabov,[51,59] Y. Riabov,[59,64] E. Richardson,[42] D. Richford,[5] T. Rinn,[25,28] N. Riveli,[55] D. Roach,[73] S. D. Rolnick,[8] M. Rosati,[28] Z. Rowan,[5] J. G. Rubin,[45] J. Runchey,[28] M. S. Ryu,[21] A. S. Safonov,[64] B. Sahlmueller,[67] N. Saito,[32] T. Sakaguchi,[7] H. Sako,[29] V. Samsonov,[51,59] M. Sarsour,[20] S. Sato,[29] S. Sawada,[32] B. Schaefer,[73] B. K. Schmoll,[69] K. Sedgwick,[8] J. Seele,[62] R. Seidl,[61,62] Y. Sekiguchi,[11] A. Sen,[20,28,69] R. Seto,[8] P. Sett,[4] A. Sexton,[42] D. Sharma,[67] A. Shaver,[28] I. Shein,[24] M. Shibata,[50] T.-A. Shibata,[61,71] K. Shigaki,[22] M. Shimomura,[28,50] T. Shioya,[72] Z. Shi,[39] K. Shoji,[61] P. Shukla,[4] A. Sickles,[7,25] C. L. Silva,[39] D. Silvermyr,[40,56] B. K. Singh,[3] V. Singh,[3]

[*] Deceased.

[†] PHENIX spokesperson: akiba@rcf.rhic.bnl.gov

M. Skolnik,[47] M. Slunečka,[9] K. L. Smith,[19,39] M. Snowball,[39] S. Solano,[47] R. A. Soltz,[38] W. E. Sondheim,[39] S. P. Sorensen,[69] I. V. Sourikova,[7] P. W. Stankus,[56] P. Steinberg,[7] E. Stenlund,[40] M. Stepanov,[43,*] A. Ster,[75] S. P. Stoll,[7] M. R. Stone,[12] T. Sugitate,[22] A. Sukhanov,[7] T. Sumita,[61] J. Sun,[67] Z. Sun,[15,67] J. Sziklai,[75] R. Takahama,[50] A. Takahara,[11] A. Taketani,[61,62] Y. Tanaka,[49] K. Tanida,[29,62,65] M. J. Tannenbaum,[7] S. Tarafdar,[3,73,74] A. Taranenko,[51,66] G. Tarnai,[15] E. Tennant,[53] R. Tieulent,[20,41] A. Timilsina,[28] T. Todoroki,[61,62,72] M. Tomášek,[14,27] H. Torii,[11] C. L. Towell,[1] R. Towell,[1] R. S. Towell,[1] I. Tserruya,[74] Y. Ueda,[22] B. Ujvari,[15] H. W. van Hecke,[39] M. Vargyas,[16,75] E. Vazquez-Zambrano,[13] A. Veicht,[13] J. Velkovska,[73] M. Virius,[14] V. Vrba,[14,27] N. Vukman,[77] E. Vznuzdaev,[59] R. Vértesi,[75] X. R. Wang,[53,62] Z. Wang,[5] D. Watanabe,[22] K. Watanabe,[61,63] Y. Watanabe,[61,62] Y. S. Watanabe,[11,32] F. Wei,[53] S. Whitaker,[28] A. S. White,[45] S. Wolin,[25] C. P. Wong,[20,39] C. L. Woody,[7] M. Wysocki,[56] B. Xia,[55] L. Xue,[20] C. Xu,[53] Q. Xu,[73] S. Yalcin,[67] Y. L. Yamaguchi,[11,67] H. Yamamoto,[72] A. Yanovich,[24] S. Yokkaichi,[61,62] I. Yoon,[65] J. H. Yoo,[33] I. Younus,[37,52] Z. You,[39] I. E. Yushmanov,[34] H. Yu,[53,58] W. A. Zajc,[13] A. Zelenski,[6] S. Zhou,[10] and L. Zou[8]

(PHENIX Collaboration)

[1]*Abilene Christian University, Abilene, Texas 79699, USA*

[2]*Department of Physics, Augustana University, Sioux Falls, South Dakota 57197, USA*

[3]*Department of Physics, Banaras Hindu University, Varanasi 221005, India*

[4]*Bhabha Atomic Research Centre, Bombay 400 085, India*

[5]*Baruch College, City University of New York, New York, New York 10010, USA*

[6]*Collider-Accelerator Department, Brookhaven National Laboratory, Upton, New York 11973, USA*

[7]*Physics Department, Brookhaven National Laboratory, Upton, New York 11973, USA*

[8]*University of California-Riverside, Riverside, California 92521, USA*

[9]*Charles University, Faculty of Mathematics and Physics, 180 00 Troja, Prague, Czech Republic*

[10]*Science and Technology on Nuclear Data Laboratory, China Institute of Atomic Energy, Beijing 102413, People's Republic of China*

[11]*Center for Nuclear Study, Graduate School of Science, University of Tokyo, 7-3-1 Hongo, Bunkyo, Tokyo 113-0033, Japan*

[12]*University of Colorado, Boulder, Colorado 80309, USA*

[13]*Columbia University, New York, New York 10027, USA and Nevis Laboratories, Irvington, New York 10533, USA*

[14]*Czech Technical University, Zikova 4, 166 36 Prague 6, Czech Republic*

[15]*Debrecen University, H-4010 Debrecen, Egyetem tér 1, Hungary*

[16]*ELTE, Eötvös Loránd University, H-1117 Budapest, Pázmány P. s. 1/A, Hungary*

[17]*Ewha Womans University, Seoul 120-750, Korea*

[18]*Florida A&M University, Tallahassee, Florida 32307, USA*

[19]*Florida State University, Tallahassee, Florida 32306, USA*

[20]*Georgia State University, Atlanta, Georgia 30303, USA*

[21]*Hanyang University, Seoul 133-792, Korea*

[22]*Physics Program and International Institute for Sustainability with Knotted Chiral Meta Matter (SKCM2), Hiroshima University, Higashi-Hiroshima, Hiroshima 739-8526, Japan*

[23]*Department of Physics and Astronomy, Howard University, Washington, DC 20059, USA*

[24]*IHEP Protvino, State Research Center of Russian Federation, Institute for High Energy Physics, Protvino 142281, Russia*

[25]*University of Illinois at Urbana-Champaign, Urbana, Illinois 61801, USA*

[26]*Institute for Nuclear Research of the Russian Academy of Sciences, prospekt 60-letiya Oktyabrya 7a, Moscow 117312, Russia*

[27]*Institute of Physics, Academy of Sciences of the Czech Republic, Na Slovance 2, 182 21 Prague 8, Czech Republic*

[28]*Iowa State University, Ames, Iowa 50011, USA*

[29]*Advanced Science Research Center, Japan Atomic Energy Agency, 2-4 Shirakata Shirane, Tokai-mura, Naka-gun, Ibaraki-ken 319-1195, Japan*

[30]*Jeonbuk National University, Jeonju 54896, Korea*

[31]*Helsinki Institute of Physics and University of Jyväskylä, P.O. Box 35, FI-40014 Jyväskylä, Finland*

[32]*KEK, High Energy Accelerator Research Organization, Tsukuba, Ibaraki 305-0801, Japan*

[33]*Korea University, Seoul 02841, Korea*

[34]*National Research Center "Kurchatov Institute," Moscow 123098, Russia*

[35]*Kyoto University, Kyoto 606-8502, Japan*

[36]*Laboratoire Leprince-Ringuet, Ecole Polytechnique, Centre National de la Recherche Scientifique IN2P3, Route de Saclay, F-91128 Palaiseau, France*

[37]*Physics Department, Lahore University of Management Sciences, Lahore 54792, Pakistan*

[38]*Lawrence Livermore National Laboratory, Livermore, California 94550, USA*

[39]*Los Alamos National Laboratory, Los Alamos, New Mexico 87545, USA*

[40]*Department of Physics, Lund University, Box 118, SE-221 00 Lund, Sweden*

[41]*IPNL, Centre National de la Recherche Scientifique IN2P3, Université Lyon, F-69622 Villeurbanne, France*

[42]*University of Maryland, College Park, Maryland 20742, USA*

[43]*Department of Physics, University of Massachusetts, Amherst, Massachusetts 01003, USA*

[44]*MATE, Laboratory of Femtoscopy, Károly Róbert Campus, H-3200 Gyöngyös, Mátraiút 36, Hungary*
[45]*Department of Physics, University of Michigan, Ann Arbor, Michigan 48109, USA*
[46]*Mississippi State University, Starkville, Mississippi 39762, USA*
[47]*Muhlenberg College, Allentown, Pennsylvania 18104, USA*
[48]*Myongji University, Yongin, Kyonggido 449-728, Korea*
[49]*Nagasaki Institute of Applied Science, Nagasaki-shi, Nagasaki 851-0193, Japan*
[50]*Nara Women's University, Kita-uoya Nishi-machi Nara 630-8506, Japan*
[51]*National Research Nuclear University, MEPhI, Moscow Engineering Physics Institute, Moscow 115409, Russia*
[52]*University of New Mexico, Albuquerque, New Mexico 87131, USA*
[53]*New Mexico State University, Las Cruces, New Mexico 88003, USA*
[54]*Physics and Astronomy Department, University of North Carolina at Greensboro, Greensboro, North Carolina 27412, USA*
[55]*Department of Physics and Astronomy, Ohio University, Athens, Ohio 45701, USA*
[56]*Oak Ridge National Laboratory, Oak Ridge, Tennessee 37831, USA*
[57]*IPN-Orsay, Univ. Paris-Sud, Centre National de la Recherche Scientifique IN2P3, Université Paris-Saclay, BP1, F-91406 Orsay, France*
[58]*Peking University, Beijing 100871, People's Republic of China*
[59]*Petersburg Nuclear Physics Institute, Gatchina, Leningrad Region 188300, Russia*
[60]*Pusan National University, Pusan 46241, Korea*
[61]*RIKEN Nishina Center for Accelerator-Based Science, Wako, Saitama 351-0198, Japan*
[62]*RIKEN BNL Research Center, Brookhaven National Laboratory, Upton, New York 11973, USA*
[63]*Physics Department, Rikkyo University, 3-34-1 Nishi-Ikebukuro, Toshima, Tokyo 171-8501, Japan*
[64]*Saint Petersburg State Polytechnic University, Saint Petersburg 195251, Russia*
[65]*Department of Physics and Astronomy, Seoul National University, Seoul 151-742, Korea*
[66]*Chemistry Department, State University of New York at Stony Brook, Stony Brook, New York 11794, USA*
[67]*Department of Physics and Astronomy, State University of New York at Stony Brook, Stony Brook, New York 11794, USA*
[68]*Sungkyunkwan University, Suwon 440-746, Korea*
[69]*University of Tennessee, Knoxville, Tennessee 37996, USA*
[70]*Texas Southern University, Houston, Texas 77004, USA*
[71]*Department of Physics, Tokyo Institute of Technology, Oh-okayama, Meguro, Tokyo 152-8551, Japan*
[72]*Tomonaga Center for the History of the Universe, University of Tsukuba, Tsukuba, Ibaraki 305, Japan*
[73]*Vanderbilt University, Nashville, Tennessee 37235, USA*
[74]*Weizmann Institute, Rehovot 76100, Israel*
[75]*Institute for Particle and Nuclear Physics, Wigner Research Centre for Physics, Hungarian Academy of Sciences, P.O. Box 49, H-1525 Budapest 114, Hungary*
[76]*Yonsei University, IPAP, Seoul 120-749, Korea*
[77]*Department of Physics, Faculty of Science, University of Zagreb, Bijenička c. 32 HR-10002 Zagreb, Croatia*
[78]*Department of Physics, School of Natural Sciences, University of Zambia, Great East Road Campus, Box 32379, Lusaka, Zambia*

(Received 18 December 2023; revised 16 March 2024; accepted 10 April 2024; published 20 May 2024)

The PHENIX experiment has performed a systematic study of identified charged-hadron ($\pi^{\pm}$, $K^{\pm}$, p, $\bar{p}$) production at midrapidity in $p+$Al, ^{3}He +Au, and Cu + Au collisions at $\sqrt{s_{NN}} = 200$ GeV and U + U collisions at $\sqrt{s_{NN}} = 193$ GeV. Identified charged-hadron invariant transverse-momentum (p_T) and transverse-mass (m_T) spectra are presented and interpreted in terms of radially expanding thermalized systems. The particle ratios of K/π and p/π have been measured in different centrality ranges of large (Cu + Au and U + U) and small ($p+$Al and ^{3}He +Au) collision systems. The values of K/π ratios measured in all considered collision systems were found to be consistent with those measured in $p+p$ collisions. However, the values of p/π ratios measured in large collision systems reach the values of $\approx$0.6, which is a factor of $\approx$2 larger than in $p+p$ collisions. These results can be qualitatively understood in terms of the baryon enhancement expected from hadronization by recombination. Identified charged-hadron nuclear-modification factors (R_{AB}) are also presented. Enhancement of proton R_{AB} values over meson R_{AB} values was observed in central ^{3}He +Au, Cu + Au, and U + U collisions. The proton R_{AB} values measured in the $p+$Al collision system were found to be consistent with R_{AB} values of ϕ, $\pi^{\pm}$, $K^{\pm}$, and π^0 mesons, which may indicate that the size of the system produced in $p+$Al collisions is too small for recombination to cause a noticeable increase in proton production.

DOI: 10.1103/PhysRevC.109.054910

I. INTRODUCTION

The quark-gluon plasma (QGP) [1,2] is a state of matter that exists at extremely high temperature and density. The QGP is composed of deconfined, strongly interacting quarks and gluons, which are ordinarily confined inside hadrons. Quantum chromodynamics, the theory of strong nuclear forces, predicts QGP formation in high-energy col-

lisions of heavy nuclei. The QGP existence has been verified by experimental observations of QGP signatures [1,3], such as strangeness enhancement [4–9], jet quenching [10–13], and baryon enhancement [14–19].

The QGP is formed in heavy ion collisions (such as Cu + Au and U + U) at temperatures larger than 300 MeV [20,21], but expands and cools down in a short time ($\approx 10\,\mathrm{fm}/c$ [3]). When the critical temperature (≈ 175 MeV [1,20]) is reached, the hadronization process begins. It was expected [20] that in relativistic ion collisions protons are produced roughly three times less than pions, reflecting the mass difference between them and the requirement for a nonzero baryon number to form a proton. Indeed, the values of the proton to pion ratio (p/π) measured by the PHENIX experiment in $p+p$ collisions do not exceed a value of 0.3. However, in central Au + Au collisions, the p/π ratio reaches a value of 0.8, indicating that protons and π mesons are produced in nearly equal proportion. The anomalous proton production observed by the PHENIX experiment [22] in Au + Au collisions at $\sqrt{s_{NN}} = 130\,\mathrm{GeV}$ [15] and later at $\sqrt{s_{NN}} = 200\,\mathrm{GeV}$ [16] was successfully described by the recombination model. The recombination model [23,24] is a hadronization model that considers hadron formation as a result of combining quarks that are nearby in phase space.

Small collision systems (such as p + Al and ^{3}He +Au) were previously studied primarily to investigate cold-nuclear-matter effects [25,26] (Cronin enhancement [27,28], multiple-parton scattering [29], and modifications of the initial nuclear-parton distribution functions [30,31]). It was thought [25,32] that the size and lifetime of the system produced in small collision systems are not sufficient for QGP formation. However, in 2019 the PHENIX experiment reported on the observation of elliptic and triangular flow patterns of charged particles produced in $p/d/^3$He +Au collisions [32]. The results of these measurements have been described in the frame of hydrodynamical models, which include the formation of short-lived QGP droplets. Comparison of identified charged-hadron production in small and large collision systems may enable systematic studies to determine the minimal conditions of QGP formation and to investigate influence of collision geometry and system size on hadron production.

This paper presents new data on identified charged-hadron production in p + Al, ^{3}He +Au, and Cu + Au collisions at $\sqrt{s_{NN}} = 200\,\mathrm{GeV}$ and U + U collisions at $\sqrt{s_{NN}} = 193\,\mathrm{GeV}$. Discussed are the influences of collision centrality and geometry on identified charged-hadron invariant p_T and m_T spectra, nuclear-modification factors, and ratios.

II. DATA ANALYSIS

The data sets used in the present analysis were collected by the PHENIX experiment during the operational periods of the Relativistic Heavy Ion Collider in calendar years 2012 (Cu + Au and U + U), 2014 (^{3}He +Au), and 2015 (p + Al). The PHENIX experiment [22] included several subdetectors that are grouped into four main blocks called arms. The central arms—east and west—cover midrapidity ($|\eta| < 0.35$) and are intended for measurement of electrons, photons, and charged hadrons. In the present analysis, the drift chambers (DCs) [33] are used for momentum determination, the time-of-flight (TOF) wall [34] is used for charged-hadron identification, and the beam-beam counters (BBCs) [35] are used for centrality determination. Detailed information about the PHENIX experiment can be found in [22,35,36].

TABLE I. Summary of the $\langle N_{\mathrm{coll}}\rangle$ and $\langle N_{\mathrm{part}}\rangle$ values calculated using Glauber Monte Carlo simulation.

System	Centrality (%)	$\langle N_{\mathrm{coll}}\rangle$	$\langle N_{\mathrm{part}}\rangle$
p + Al	0–72	2.1 ± 0.2	3.1 ± 0.1
	0–20	3.4 ± 0.3	4.4 ± 0.3
	20–40	2.3 ± 0.2	3.3 ± 0.1
	40–72	1.7 ± 0.1	1.6 ± 0.2
^{3}He +Au	0–88	10.4 ± 0.7	11.3 ± 0.5
	0–20	22.3 ± 1.7	21.1 ± 1.3
	20–40	14.8 ± 1.1	15.4 ± 0.9
	40–60	8.4 ± 0.6	9.5 ± 0.6
	0–88	3.4 ± 0.3	4.8 ± 0.3
Cu + Au	0–80	123.8 ± 12.0	70.4 ± 3.0
	0–20	313.8 ± 28.4	154.8 ± 4.1
	20–40	129.3 ± 12.4	80.4 ± 3.3
	40–60	41.8 ± 5.3	34.9 ± 2.9
	60–80	10.1 ± 2.0	11.5 ± 1.8
U + U	0–80	342 ± 30	143 ± 5
	0–20	935 ± 98	330 ± 6
	20–40	335 ± 33	259 ± 7
	40–60	81 ± 13	65 ± 6
	60–80	17 ± 4	18 ± 3

A. Event selection

The minimum-bias (MB) trigger was used for event selection. The MB trigger selects events that correspond to simultaneous signals in the north (forward rapidity) and south (backward rapidity) BBC detectors. The collision vertex coordinate is required to be $|z_{\mathrm{vtx}}| < 30\,\mathrm{cm}$ relative to the center of the spectrometer. Determination of centrality in the PHENIX experiment is done with the BBC according to the procedure described in [37]. The numbers of participating nucleons $\langle N_{\mathrm{part}}\rangle$ as well as numbers of binary nucleon-nucleon collisions $\langle N_{\mathrm{coll}}\rangle$ are calculated using Glauber Monte Carlo (MC) simulations. The $\langle N_{\mathrm{part}}\rangle$ and $\langle N_{\mathrm{coll}}\rangle$ values are presented in Table I.

B. Particle identification

Charged hadrons are detected in the TOF wall and the DC of the PHENIX experiment. The squared mass of tracks can be determined in accordance with Eq. (1):

$$m^2 = \frac{p^2}{c^2}\left(\frac{t^2c^2}{L^2} - 1\right), \tag{1}$$

where p is the momentum of the particle measured with the DC, L is the particle flight path length from the event vertex to the TOF detector, t is the time of flight measured in TOF detector, and c is the speed of light [36]. Table II presents p_T ranges of identified charged-hadron-yield measurements.

TABLE II. The p_T ranges (GeV/c) of identified charged-hadron yields measurements.

Hadron	$p+$Al	^{3}He$+$Au	Cu$+$Au	U$+$U
π^+	0.5–2.0	0.5–3.0	0.5–3.0	0.5–3.0
π^-	0.5–2.0	0.5–3.0	0.5–3.0	0.5–3.0
K^+	0.5–1.8	0.5–2.0	0.5–2.0	0.5–2.0
K^-	0.5–1.8	0.5–2.0	0.5–2.0	0.5–2.0
p		0.5–4.0	0.5–4.0	0.5–4.0
$\bar{p}$	0.5–2.5	0.5–4.0	0.5–4.0	0.5–4.0

The distribution of m^2 multiplied by charge versus transverse momentum (p_T) as found from TOF timing, DC momentum, and the path length is presented in Fig. 1. Signals corresponding to $\pi^{\pm}$, $K^{\pm}$, and p and $\bar{p}$ are clearly distinguishable. In $p+$Al collisions, the proton sample has a large contamination of spallation protons from the inner silicon detectors. For that reason, they are excluded from measurements that require absolute normalization, like the spectra, ratios, and nuclear modification factors reported in this paper.

Particle identification (PID) was carried out by applying two-standard-deviation (2σ) PID cuts in m^2 and momentum space for each particle species. The hadron's signals from TOF are approximated by Gaussian functions with the root-mean-square deviations ($\sigma_{\rm TOF}$) and mathematical expectations ($m^2_{\rm TOF}$) in every $\Delta p_T = 0.5$ GeV/c interval of the hadron identification p_T range from Table II. Discrete $\sigma_{\rm TOF}(p_T)$ and $m^2_{\rm TOF}(p_T)$ dependencies are parametrized by Eq. (2). PID cuts are based on obtained continuous functions $\sigma_{\rm TOF}(p_T)$ and $m^2_{\rm TOF}(p_T)$, which are presented in Fig. 1 with black solid lines.

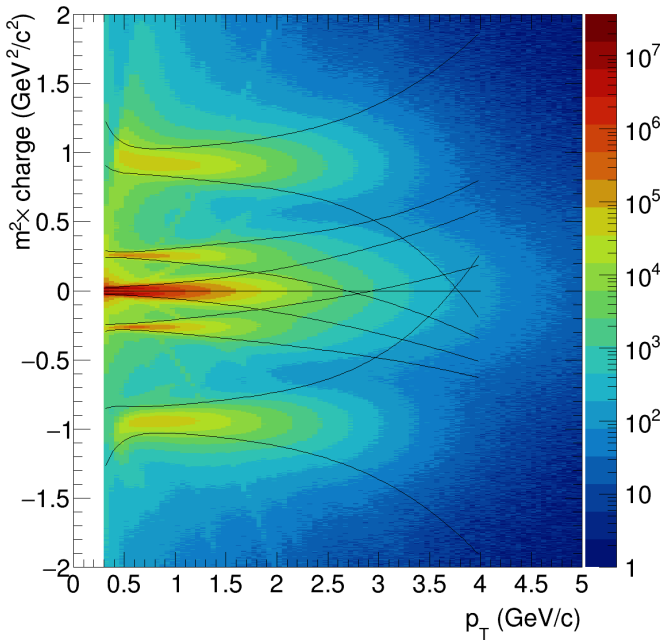

FIG. 1. Distribution of hadron squared mass multiplied by charge ($m^2 \times$ charge) vs hadron p_T as found from TOF timing, DC momentum, and the path length. Black solid lines represent PID cuts, based on Eq. (2), which were used for hadron identification.

The fit to both the mean $m^2_{\rm TOF}(p_T)$ and the standard deviation $\sigma_{\rm TOF}(p_T)$ uses the same functional form:

$$m^2_{\rm TOF}(p_T), \sigma_{\rm TOF}(p_T) = p_0 + \frac{p_1}{p_T} + \frac{p_2}{p_T^2} + p_3 e^{\sqrt{p_T}} + p_4\sqrt{p_T}, \tag{2}$$

where p_0, p_1, p_2, p_3, and p_4 are fit parameters, and the set of fit parameters is different for $m^2_{\rm TOF}(p_T)$ and $\sigma_{\rm TOF}(p_T)$. In the high-p_T region, hadron signals start to overlap; therefore, the veto cut was introduced for better separation of π, K, and p. The veto cut requires that the hadron mass does not satisfy the $1.5\,\sigma$ condition for neighboring hadrons. The PID and veto cuts are standard for the PHENIX detector [14,17].

C. Corrections to the raw data

The measured values of identified charged-hadron primary yields should be corrected for the geometric acceptance of the detectors, detector efficiency, and analysis cuts used in data selection [14,17]. This section describes procedures of estimating the corrections applied to the raw identified charged-hadron yields.

1. Reconstruction efficiency

The geometric acceptance of the detectors, detector efficiency, and analysis cuts have been taken into account by the reconstruction efficiency factor ($\epsilon_{\rm rec}$), estimated using a single-particle MC simulation. The MC simulation was carried out using the PHENIX integrated simulation application (PISA) package [38], which is based on GEANT3 [39] simulation software. In the PISA project the geometry, material, spatial, momentum, and energy resolutions of the PHENIX detector subsystems as well as the configuration of the magnetic field are simulated in full accordance with the structure of the real facility. Simulated events have been processed using the same analysis criteria as the data. In that way, the reconstruction efficiency $\epsilon_{\rm rec}(p_T)$ can be estimated by the number of reconstructed hadrons ($N^{\rm MC}_{\rm rec}$) divided by the total number of hadrons generated in the MC model ($N^{\rm MC}_{\rm tot}$):

$$\epsilon_{\rm rec}(p_T) = \frac{dN^{\rm MC}_{\rm rec}/dp_T}{dN^{\rm MC}_{\rm tot}/dp_T}. \tag{3}$$

2. Weak-decay correction

Hyperon weak decays are an additional source of contamination for p and $\bar{p}$ yields. The fraction of detected p and $\bar{p}$ that come from hyperon weak decays can be taken into account by feed-down corrections $C_{\rm FD} = 1 - \delta_{\rm FD}$, where $\delta_{\rm FD}$ is determined as a fraction of p (or $\bar{p}$) that come from hyperon weak decays to the total number of registered protons (antiprotons). The greatest contribution to the amount of decay protons and antiprotons is made by Λ and $\bar{\Lambda}$ decays [14]. The contribution of Σ^0 is implicitly taken into account when considering Λ and $\bar{\Lambda}$ decays, because Σ^0 decays electromagnetically with 100% branching ratio to Λ and a photon. Other weak hyperon decays, such as $\Sigma^{\pm}$ and Ξ, have not been considered in the present analyses. The contribution of charged Σ states, Ξ and Ω multistrange baryon states, is small [17,37] and was included in the overall systematic uncertainty estimates.

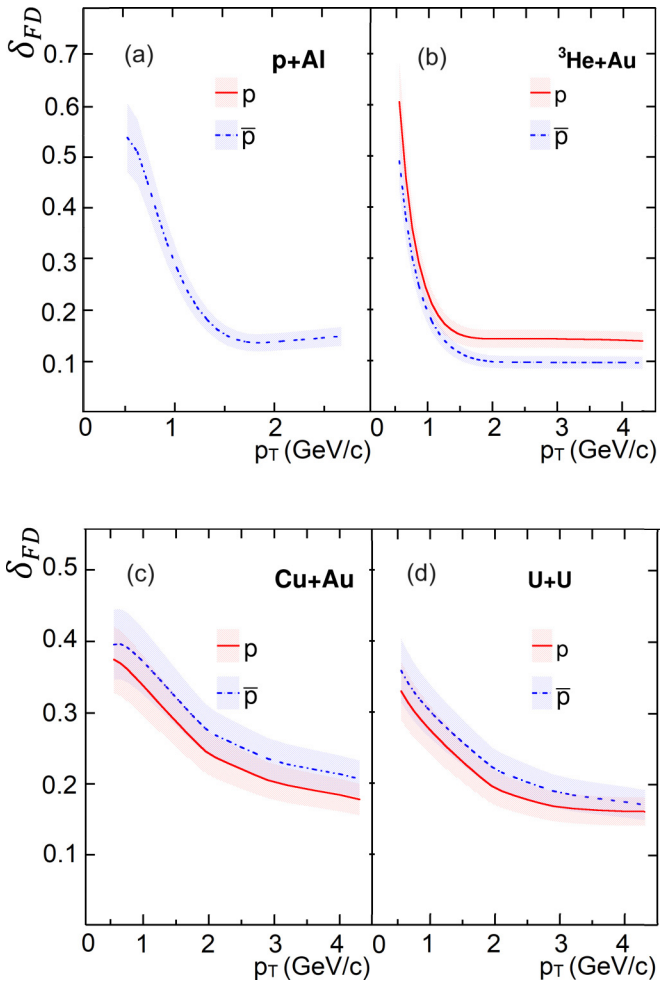

FIG. 2. $\delta_{\rm FD}$ values as a function of p_T for protons and antiprotons, measured in $p+$Al, ^{3}He$+$Au, Cu$+$Au, and U$+$U collisions. The shaded bands indicate the systematic uncertainty.

MC simulations of Λ and $\bar{\Lambda}$ are used to calculate the fraction of p and $\bar{p}$ that come from Λ and $\bar{\Lambda}$ decays. Figure 2 shows the values of $\delta_{\rm FD}$ as a function of p_T, obtained in $p+$Al, ^{3}He$+$Au, Cu$+$Au, and U$+$U collisions.

3. Bias-factor correction

The MB trigger is biased for events with high multiplicity, leading to miscalculations of hadron invariant yields in small collision systems [40]. The bias of the MB trigger arises mostly from single- and double-diffractive events, which result in particle production very close to the beam line. The BBC trigger is therefore biased to the nondiffractive collisions, which have larger particle production at midrapidity. In such cases, there will exist a bias towards higher charge deposition in the BBC and, hence, towards larger centrality [40]. The bias effect was corrected by applying bias-factor corrections ($f_{\rm bias}$). The values of $f_{\rm bias}$ corrections are estimated with the help of Glauber MC simulations and presented in Table III.

TABLE III. Summary of the $f_{\rm bias}$ correction values calculated using Glauber Monte Carlo simulation.

Collision system	Centrality (%)	$f_{\rm bias}$
$p+$Al	0–72	0.80 ± 0.02
	0–20	0.81 ± 0.01
	20–40	0.90 ± 0.02
	40–72	1.05 ± 0.04
^{3}He$+$Au	0–88	0.89 ± 0.01
	0–20	0.95 ± 0.01
	20–40	1.01 ± 0.01
	40–60	1.02 ± 0.01
	60–88	1.03 ± 0.05

D. Systematic uncertainties

Systematic uncertainties are divided into three types: type *A*, type *B*, and type *C*. Uncertainties of type *A* are point-to-point uncorrelated in transverse momentum and centrality. Type *B* uncertainties are point-to-point correlated with transverse momentum. Type *A* and *B* uncertainties arise as a result of acceptance uncertainties, weak decay correction uncertainty, applying track selection, and PID cuts. The values of type *A* and *B* uncertainties have been estimated by varying analysis-cut parameters. Track selection and acceptance uncertainties mostly cancel for measurements of p/π and K/π ratios [14,17], so only uncertainties associated with PID cuts and weak decay correction are shown with the results presented in Table IV.

Uncertainties of type *C* are fully correlated in transverse momentum, i.e., uncertainties of type *C* shift hadron yields equally in the entire range of the transverse momentum. In this paper, the type *C* uncertainties are attributed to the uncertainty in estimation of $\langle N_{\rm coll}\rangle$ and $f_{\rm bias}$ values.

E. Invariant spectra

The $\pi^{\pm}$, $K^{\pm}$, p, and $\bar{p}$ invariant transverse momentum spectra were measured in $p+$Al, ^{3}He$+$Au, and Cu$+$Au collisions at $\sqrt{s_{NN}} = 200$ GeV and in U$+$U collisions at $\sqrt{s_{NN}} = 193$ GeV as follows:

$$\frac{1}{2\pi p_T}\frac{d^2N}{dp_T dy} = \frac{1}{2\pi p_T}\frac{N_h f_{\rm bias} C_{\rm FD}}{N_{\rm evt}\varepsilon_{\rm rec}\Delta p_T \Delta y}, \tag{4}$$

where N_h is the raw yield of hadron h, $N_{\rm evt}$ is the number of nucleus-nucleus collisions, y is rapidity, $C_{\rm FD}$ is the feed-down correction, and $f_{\rm bias}$ is the bias-factor correction. $C_{\rm FD} = 1$ for $\pi^{\pm}$ and $K^{\pm}$; $f_{\rm bias} = 1$ for the large collision systems. The resulting $\pi^{\pm}$, $K^{\pm}$, p, and $\bar{p}$ invariant p_T spectra are presented in Fig. 3.

The π, K, and p invariant p_T spectra exhibit different shapes. To quantify these differences, invariant-transverse-mass ($m_T = \sqrt{p_T^2 + m_0^2}$) spectra were calculated. The m_T invariant spectra of all identified charged hadrons have exponential form for $m_T < 1.5$ GeV and can be approximated by

TABLE IV. Values of type *A* uncertainties summed quadratically to the values of type *B* uncertainties (%) on the identified charged-hadron invariant yields and ratios. The p_T ranges correspond to Table II.

		p_T (GeV/c)				
System	Hadron	0.5–1%	1–1.5%	1.5–2.0%	2.0–3.0%	3.0–4.0%
$p+$Al	π^+	9.7	10.5	11.3		
	π^-	8.7	11.0	10.5		
	K^+	7.9	10.2	13.7		
	K^-	7.7	9.9	15.0		
	$\bar{p}$	9.3	7.9	7.7	8.8	
	K^+/π^+	3.6	3.9	8.1		
	K^-/π^-	3.6	3.7	8.7		
	$\bar{p}/\pi^-$	6.0	6.1	6.6	6.6	
^{3}He$+$Au	π^+	5.7	4.2	5.7	6.7	
	π^-	11.6	11.3	10.5	9.1	
	K^+	8.3	8.6	10.0		
	K^-	8.7	9.9	11.3		
	p	8.6	8.6	8.8	8.5	8.8
	$\bar{p}$	9.1	10.0	10.4	10.3	10.6
	K^+/π^+	5.1	4.0	5.1		
	K^-/π^-	5.0	4.0	5.2		
	p/π^+	7.1	6.4	7.2	7.8	
	$\bar{p}/\pi^-$	7.2	6.4	6.5	7.9	
Cu$+$Au	π^+	10.2	10.9	10.5	9.9	
	π^-	8.9	10.1	10.0	10.5	
	K^+	10.2	8.3	7.5		
	K^-	10.0	7.7	8.6		
	p	10.3	11.5	12.4	13.1	16.5
	$\bar{p}$	8.4	8.6	10.3	10.9	12.8
	K^+/π^+	7.0	7.0	7.7		
	K^-/π^-	7.2	7.2	8.0		
	p/π^+	8.5	8.6	10.0	10.1	
	$\bar{p}/\pi^-$	9.1	8.5	8.7	8.7	
U$+$U	π^+	16.8	16.5	14.7	13.7	
	π^-	6.2	8.8	9.4	16.9	
	K^+	10.2	8.3	8.3		
	K^-	8.8	7.6	8.5		
	p	10.0	9.8	9.8	11.2	14.1
	$\bar{p}$	10.3	10.0	9.1	10.5	15.2
	K^+/π^+	6.9	7.0	7.4		
	K^-/π^-	8.0	7.0	7.8		
	p/π^+	9.0	8.5	9.0	8.6	
	$\bar{p}/\pi^-$	10.0	9.6	9.0	9.2	

Eq. (5) [14]:

$$\frac{1}{2\pi m_T}\frac{d^2N}{dm_T dy} = \frac{A}{2\pi T(T+m_0)}\exp\left(-\frac{m_T-m_0}{T}\right) \quad (5)$$

where T is the inverse-slope parameter and A is a normalization factor. Examples of resulting π^+, K^+, and p invariant-m_T spectra measured in central Cu $+$ Au collisions are presented in Fig. 4. Approximations by Eq. (5) are shown with (red) solid lines. Values of inverse-slope parameters T calculated in $p+$Al, ^{3}He$+$Au, Cu $+$ Au, and U $+$ U collisions are summarized in Table V.

Figure 5 shows examples of T parameter vs hadron mass (m_0) dependencies for different centralities of Cu $+$ Au collisions. Ordering of pion, kaon, and proton inverse slope values $T_\pi < T_K < T_p$ can be seen in all centralities.

The difference between T values, calculated for protons in central and peripheral U $+$ U collisions, is 18% and decreases from large to small collision systems. The T values, calculated for pions in different centralities, are nearly of the same values in all collision systems. The T values, calculated for kaons, take intermediate values between pion and proton T-parameter values. Description of hadron p_T spectra shape and parameter T dependence on hadron mass, collision system size, and centrality can be given by thermal models [14,41,42]. Thermal models consider a thermalized system with a well-defined temperature and a common transverse velocity field. Under the assumption of complete decoupling between the thermal and collective motion of the particles, the hadron kinetic energy ($\langle E_{\rm kinetic}\rangle$) is equal to the linear sum of the energy of the thermal motion ($\langle E_{\rm thermal}\rangle$) and the energy of the collective motion ($\langle E_{\rm collective}\rangle$), $\langle E_{\rm kinetic}\rangle = \langle E_{\rm thermal}\rangle + \langle E_{\rm collective}\rangle$. For that reason, the inverse-slope parameter T exhibits mass dependence given by

$$T = T_0 + m\langle u_t\rangle^2, \quad (6)$$

where T_0 can be interpreted as a freeze-out temperature and $\langle u_t\rangle$ as the average collective velocity for all particle species.

III. RESULTS

The dotted lines on Fig. 5 represent linear fits of the $T(m_0)$ values from each centrality bin by Eq. (6). The fit parameters for positively charged (T_0^+, $\langle u_t\rangle^+$) and negatively charged (T_0^-, $\langle u_t\rangle^-$) hadrons calculated in $p+$Al, ^{3}He$+$Au, Cu $+$ Au, and U $+$ U collision systems are shown in the Table VI and presented in Figs. 6 and 7 as a function of $\langle N_{\rm part}\rangle$ values. Presented error values for $T_0^\pm$ and $\langle u_t\rangle^\pm$ parameters are due to the fit uncertainties. The T_0 values calculated in collisions with different geometries and centralities were found to be coincident within uncertainties, indicating that the freeze-out temperature is approximately independent of $\langle N_{\rm part}\rangle$ values. The averaged T_0 value was found to be 166.1 ± 2.2 MeV, which is shown as the (red) solid line in Fig. 6. In contrast, the strength of the average transverse flow ($\langle u_t\rangle$ values) increases from small to large $\langle N_{\rm part}\rangle$ values, supporting the hydrodynamic picture. The $\langle u_t\rangle(\langle N_{\rm part}\rangle)$ values were approximated with the fit function $p_1\log(p_2\langle N_{\rm part}\rangle)$, where $p_1 = 0.0345\pm0.0003$ and $p_2 = 3196\pm342$. These fit parameters could provide insight into theoretical models for radially expanding thermalized systems.

A. Particle ratios

Enhancement of baryon production in nucleus-nucleus collisions is considered to be one of the signatures of QGP formation [14,15,17]. To investigate differences in baryon and meson production mechanisms, the ratios of p/π and K/π have been calculated. Figures 8 and 9 present comparisons of p/π^+ and $\bar{p}/\pi^-$ ratios in different centralities of large (Cu $+$ Au and U $+$ U) and small ($p+p$, $p+$Al, and ^{3}He$+$Au) collision systems. In central collisions of large systems p/π ratios reach the values of $\approx$0.6, but in peripheral collisions the values of p/π ratios are smaller than 0.4 in the whole

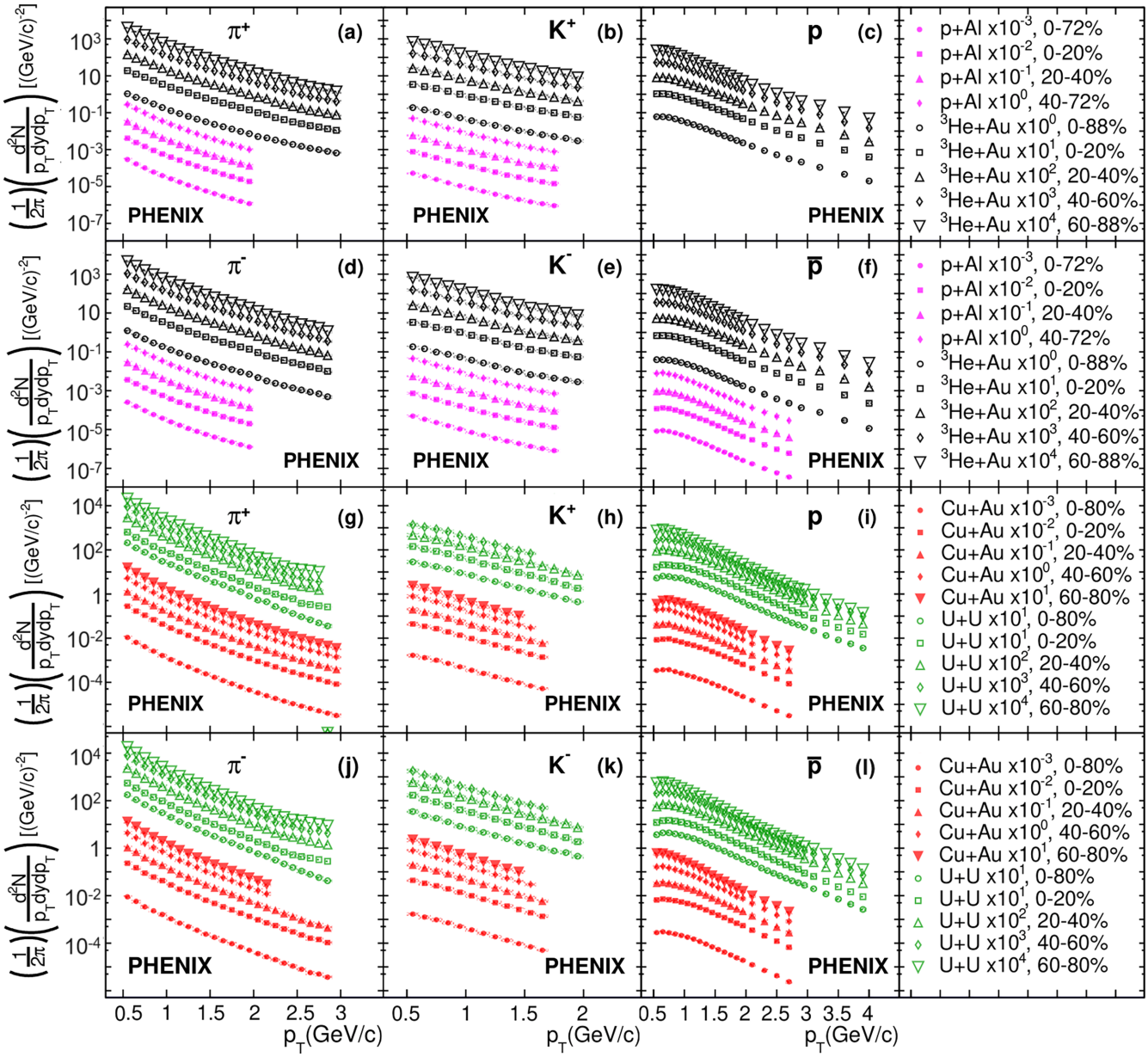

FIG. 3. The π^+, π^-, K^+, K^-, p, and $\bar{p}$ invariant p_T spectra measured in different centralities of $p+$Al, ^{3}He +Au, and Cu + Au collisions at $\sqrt{s_{NN}} = 200$ GeV and U + U collisions at $\sqrt{s_{NN}} = 193$ GeV. Invariant p_T spectra are multiplied by powers of 10 for clarity of presentation.

p_T range. Behavior of p/π ratios observed in Cu + Au and U + U collision systems can be qualitatively described using recombination models [23,24].

In small collision systems ($p+$Al and ^{3}He +Au), the values of p/π ratios are similar to those measured in $p+p$ collisions [43]. In ^{3}He +Au collisions a modest centrality dependence can be seen, similar to that observed in $d+$Au collisions [14,17]. The modest centrality dependence can be understood in terms of the small range of $\langle N_{\rm part}\rangle$ values relative to the large range of $\langle N_{\rm part}\rangle$ values in large collision systems. The values of p/π ratios measured in all centrality classes of $p+$Al collisions and in $p+p$ collisions are consistent within uncertainties. For all measurements type A uncertainties sum quadratically to type B uncertainties and are shown as a rectangles around the experimental points in Figs. 10–15.

The ratios of K^+/π^+ and K^-/π^- are shown in Figs. 10 and 11. The values of K/π ratios show a modest centrality dependence, which is insignificant within systematic uncertainties. The centrality dependence of K/π ratios in $d+$Au and Au + Au collisions was attributed to a strangeness-enhancement effect [17].

B. Nuclear-modification factors

To quantify differences of hadron production in relativistic nucleus-nucleus collisions ($A+B$) and in $p+p$ collisions, nuclear modification factors (R_{AB}) were calculated

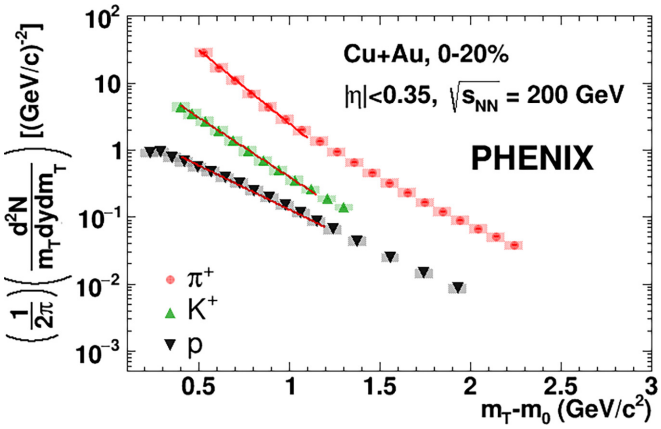

FIG. 4. An example of π^+, K^+, and p invariant m_T spectra measured in central Cu + Au collisions at $\sqrt{s_{NN}} = 200$ GeV. Approximations with Eq. (5) are presented with red solid lines.

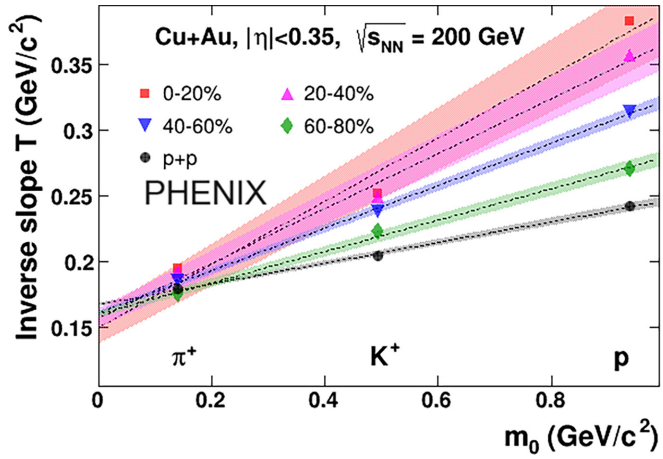

FIG. 5. Mass and centrality dependence of inverse slope parameters T for π^+, K^+, and p in Cu + Au collisions at $\sqrt{s_{NN}} = 200$ GeV. The dotted lines represent linear fits of the $T(m_0)$ values from each centrality bin by Eq. (6). The T values measured for π^+, K^+, and p in $p + p$ collisions are shown for comparison.

as follows:

$$R_{AB} = \frac{1}{\langle N_{\rm coll}\rangle} \frac{d^2N_{A+B}/dp_T dy}{d^2N_{p+p}/dp_T dy}, \tag{7}$$

where $d^2N_{A+B}/dp_T dy$ and $d^2N_{p+p}/dp_T dy$ are the invariant spectra measured in $A + B$ and $p + p$ collisions, respectively.

Figures 12 and 13 present comparisons of identified charged-hadron R_{AB} values as a function of p_T in central and peripheral $p + $ Al, ^{3}He +Au, Cu + Au, and U + U collisions. The R_{AB} values are found to be in agreement in collisions with different geometries, but with the same $\langle N_{\rm part}\rangle$ values, indicating that identified charged-hadron production depends only on system size and not geometry.

The following features of identified charged-hadron production in $p + $ Al collisions have been found: (i) the slope of $R_{AB}(p_T)$ in $p + $ Al collisions is flatter than it is in ^{3}He +Au and $d + $ Au collisions and (ii) proton R_{AB} values in $p + $ Al collisions at the intermediate p_T range ($1.0 < p_T < 2.5$ GeV/c) are equal to unity, while in ^{3}He +Au and $d + $ Au collisions proton R_{AB} is above unity. Differences in identified charged-hadron production between $p + $ Al and $d/^3$He +Au might be caused by the size of the $p + $ Al system being insufficient to observe an increase in proton production.

Comparisons of identified charged-hadron R_{AB} values with neutral-meson R_{AB} values [44,45,47] in small and large collision systems are presented in Figs. 14 and 15. In large collision systems and in the ^{3}He +Au collision system, proton R_{AB} values are enhanced over all meson R_{AB} values. The mass of the ϕ-meson $m_\phi = 1019\,\text{MeV}/c^2$ is similar to the proton mass $m_p = 938\,\text{MeV}/c^2$, therefore the enhancement of proton

TABLE V. Identified charged-hadron inverse slope parameters T (MeV/c^2) calculated in $p + $ Al, ^{3}He +Au, Cu + Au, and U + U collision systems.

System	$\langle N_{\rm part}\rangle$	π^+	π^-	K^+	K^-	p	$\bar{p}$
$p + $ Al	3.1 ± 0.1	178.88 ± 0.35	187.36 ± 0.18	210.69 ± 0.77	206.61 ± 0.78		269.51 ± 1.25
	4.4 ± 0.3	183.83 ± 0.28	192.56 ± 0.29	216.10 ± 1.22	211.25 ± 1.21		275.14 ± 1.16
	3.3 ± 0.1	178.20 ± 0.32	186.96 ± 0.33	210.05 ± 1.43	206.25 ± 1.46		266.62 ± 2.28
	1.6 ± 0.2	173.88 ± 0.46	181.99 ± 0.26	204.74 ± 1.16	201.47 ± 1.18		254.20 ± 1.82
^{3}He +Au	11.3 ± 0.5	208.70 ± 0.07	187.25 ± 0.06	235.84 ± 0.24	236.98 ± 0.25	295.74 ± 0.20	303.59 ± 0.24
	21.1 ± 1.3	214.33 ± 0.11	191.58 ± 0.09	242.57 ± 0.38	242.91 ± 0.39	309.27 ± 0.33	317.40 ± 0.76
	15.4 ± 0.9	209.84 ± 0.13	188.33 ± 0.10	237.27 ± 0.44	238.49 ± 0.46	296.44 ± 0.37	295.10 ± 0.18
	9.5 ± 0.6	202.71 ± 0.15	182.66 ± 0.13	227.37 ± 0.53	229.34 ± 0.55	280.01 ± 0.44	287.12 ± 0.54
	4.8 ± 0.3	191.01 ± 0.18	172.40 ± 0.15	213.44 ± 0.66	215.99 ± 0.70	254.22 ± 0.55	261.83 ± 0.66
Cu + Au	70.4 ± 3.0	191.72 ± 0.01	205.41 ± 0.01	249.33 ± 0.03	253.80 ± 0.03	363.65 ± 0.09	344.75 ± 0.08
	154.8 ± 4.1	194.29 ± 0.12	208.57 ± 0.01	251.43 ± 0.04	255.85 ± 0.09	383.85 ± 0.13	365.18 ± 0.13
	80.4 ± 3.3	192.07 ± 0.02	205.67 ± 0.02	249.14 ± 0.06	253.34 ± 0.05	357.54 ± 0.16	338.92 ± 0.15
	34.9 ± 1.8	185.32 ± 0.03	197.72 ± 0.03	238.05 ± 0.09	243.35 ± 0.09	313.90 ± 0.20	306.48 ± 0.20
	11.5 ± 1.8	175.24 ± 0.05	186.06 ± 0.05	222.76 ± 0.18	228.90 ± 0.18	270.86 ± 0.28	263.38 ± 0.29
U + U	330 ± 6	198.18 ± 0.02	205.84 ± 0.21	266.49 ± 0.08	265.80 ± 0.08	382.54 ± 0.19	374.48 ± 0.21
	259 ± 7	197.28 ± 0.04	202.39 ± 0.03	269.42 ± 0.12	266.36 ± 0.11	358.24 ± 0.23	353.94 ± 0.26
	65 ± 6	192.42 ± 0.06	197.74 ± 0.06	259.69 ± 0.22	257.80 ± 0.20	314.92 ± 0.32	308.57 ± 0.35

TABLE VI. Freeze-out temperatures and averaged collective velocities calculated for positively charged (T_0^+, $\langle u_t\rangle^+$) and negatively charged (T_0^-, $\langle u_t\rangle^-$) hadrons at different centralities of $p+$Al, ^{3}He$+$Au, Cu $+$ Au, and U $+$ U collisions.

System	$\langle N_{\rm part}\rangle$	T_0^+	T_0^-	$\langle u_t\rangle^+$	$\langle u_t\rangle^-$
$p+$Al	3.1 ± 0.1	167.99 ± 2.17	166.49 ± 15.29	0.28 ± 0.01	0.32 ± 0.04
	4.4 ± 0.3	171.84 ± 0.92	171.33 ± 15.96	0.29 ± 0.01	0.32 ± 0.04
	3.3 ± 0.1	168.01 ± 2.15	167.88 ± 14.30	0.28 ± 0.01	0.31 ± 0.04
	1.6 ± 0.2	164.10 ± 4.39	163.80 ± 11.20	0.27 ± 0.01	0.30 ± 0.03
^{3}He$+$Au	11.3 ± 0.5	189.16 ± 10.22	166.27 ± 1.70	0.33 ± 0.03	0.38 ± 0.01
	21.1 ± 1.3	193.84 ± 12.42	166.44 ± 3.23	0.34 ± 0.03	0.39 ± 0.01
	15.4 ± 0.9	188.99 ± 9.82	167.59 ± 1.24	0.33 ± 0.02	0.38 ± 0.01
	9.5 ± 0.6	185.05 ± 8.57	164.60 ± 0.27	0.31 ± 0.02	0.36 ± 0.01
	4.8 ± 0.3	177.02 ± 4.99	158.33 ± 3.45	0.28 ± 0.01	0.33 ± 0.01
Cu $+$ Au	70.4 ± 3.0	154.06 ± 16.63	176.03 ± 11.95	0.46 ± 0.03	0.41 ± 0.02
	154.8 ± 4.1	149.99 ± 23.98	172.82 ± 19.75	0.48 ± 0.05	0.44 ± 0.04
	80.4 ± 3.3	157.02 ± 14.55	178.11 ± 10.20	0.45 ± 0.03	0.40 ± 0.02
	34.9 ± 2.9	161.02 ± 3.86	177.79 ± 2.35	0.40 ± 0.01	0.36 ± 0.01
	11.5 ± 1.8	160.04 ± 4.50	175.86 ± 7.56	0.34 ± 0.01	0.30 ± 0.02
U $+$ U	330 ± 6	160.03 ± 12.02	170.80 ± 13.24	0.48 ± 0.02	0.46 ± 0.03
	259 ± 7	169.04 ± 0.60	174.76 ± 2.93	0.44 ± 0.01	0.43 ± 0.01
	65 ± 6	176.03 ± 11.45	182.61 ± 9.64	0.39 ± 0.02	0.37 ± 0.02

R_{AB} values over ϕ-meson R_{AB} values suggests differences in baryon versus meson production instead of a simple mass dependence. In $p+$Al collisions proton R_{AB} values and R_{AB} values of all measured mesons are in agreement within uncertainties, which shows zero enhancement in proton to ϕ-meson production.

The p/π^+ and $\bar{p}/\pi^-$ ratios integrated in the low-p_T (high-p_T) regions, $p_T < 1.5$ GeV/c ($p_T > 1.5$GeV/c), are plotted in Fig. 16 as a function of $\langle N_{\rm part}\rangle$. The values of ratios, integrated in the low-p_T region [Figs. 16(a) and 16(c)], were found to be approximately independent of $\langle N_{\rm part}\rangle$ values. The values of ratios, integrated in the high-p_T region [Figs. 16(b) and 16(d)], smoothly grow with increasing $\langle N_{\rm part}\rangle$. Because the $\bar{p}/p$ ratio is approximately equal to 0.73 [14], regardless of $\langle N_{\rm part}\rangle$ the integrated p/π^+ ratios exceed the integrated $\bar{p}/\pi^-$ ratios.

According to the recombination model, the p_T of a produced hadron is the sum of the p_T of its constituent quarks. Therefore, baryon-invariant p_T spectra are shifted towards larger p_T relative to the meson p_T spectra, which leads to an enhancement in baryon over meson production in the intermediate p_T region. Therefore, the behavior of the integrated ratio supports the assumption that the influence of the recombination mechanism grows with increasing $\langle N_{\rm part}\rangle$.

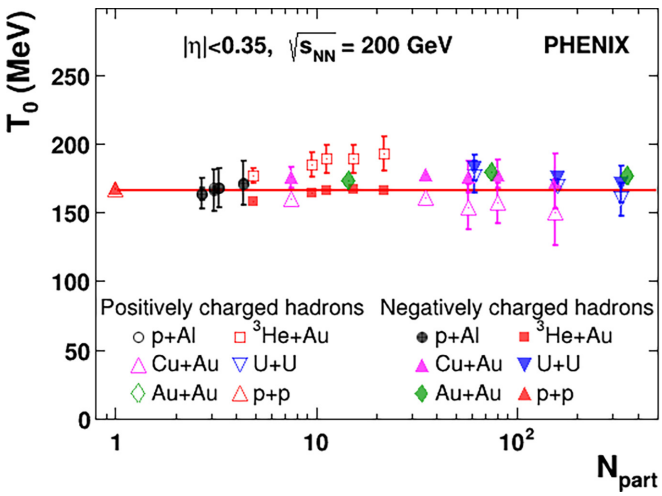

FIG. 6. Freeze-out temperature (T_0) as a function of $\langle N_{\rm part}\rangle$ obtained for positively and negatively charged hadrons at different centralities of $p+$Al, ^{3}He$+$Au, Cu $+$ Au, and U $+$ U collisions. The T_0 values measured in $p+p$ collisions are shown for comparison.

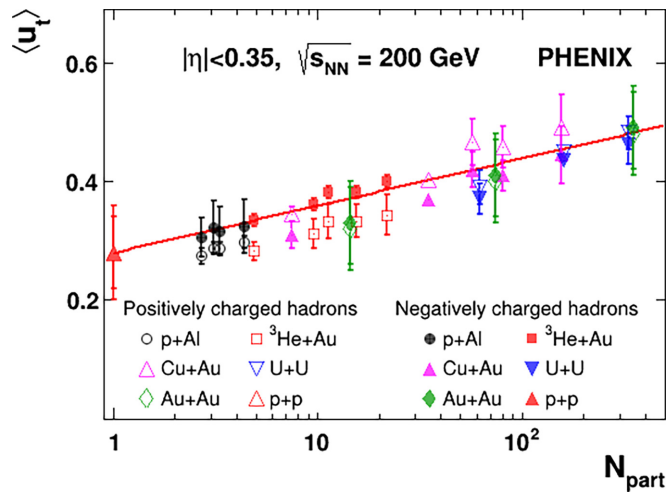

FIG. 7. Collective velocities ($\langle u_t\rangle$) as a function of $\langle N_{\rm part}\rangle$ obtained for positively and negatively charged hadrons in different centralities of $p+$Al, ^{3}He$+$Au, Cu $+$ Au, and U $+$ U collisions. The $\langle u_t\rangle$ values measured in $p+p$ collisions are shown for comparison.

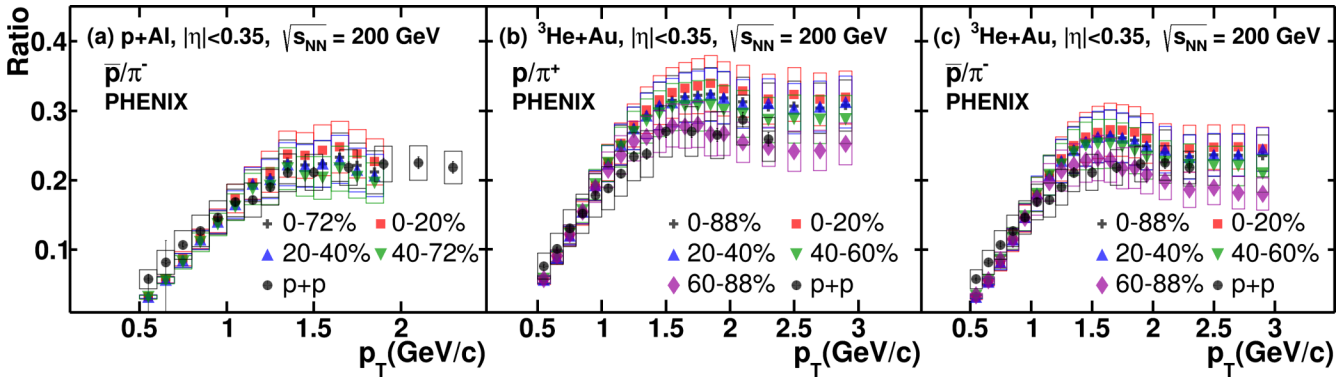

FIG. 8. The ratios of p/π^+ as a function of p_T measured in different centralities of ^{3}He +Au collisions and $\bar{p}/\pi^-$ ratios measured in different centralities of p + Al and ^{3}He +Au collisions. Data points, measured in $p+p$ collisions [43], are shown as a comparison.

IV. SUMMARY

The PHENIX experiment has measured identified charged-hadron invariant p_T and m_T spectra and nuclear-modification factors R_{AB}, and p/π and K/π ratios in p + Al, ^{3}He +Au, and Cu + Au collisions at $\sqrt{s_{NN}} = 200$ GeV and in U + U collisions at $\sqrt{s_{NN}} = 193$ GeV.

The values of freeze-out temperatures T_0 and average collective velocities $\langle u_t \rangle$ have been obtained. The T_0 values do not exhibit any dependence on the collision centrality and $\langle N_{\rm part} \rangle$ values, whereas the values of $\langle u_t \rangle$ smoothly increase with increasing of $\langle N_{\rm part} \rangle$ values. This indicates that in collisions characterized by large $\langle N_{\rm part} \rangle$ values (central Cu + Au, Au + Au, and U + U collisions), collective effects are more pronounced than in collision systems with small $\langle N_{\rm part} \rangle$ values (p + Al and ^{3}He +Au collisions and peripheral collisions of large systems).

The p/π and K/π ratios have been measured to investigate differences in baryon vs meson production in large and small collision systems. In collisions with small $\langle N_{\rm part} \rangle$ values the ratios of p/π are comparable to those measured in $p+p$ collisions ($(p/\pi)^{p+p}$). In collision systems with large $\langle N_{\rm part} \rangle$ values p/π ratios reach the values of $\approx$0.6, which is a factor of $\approx$2 larger than $(p/\pi)^{p+p}$.

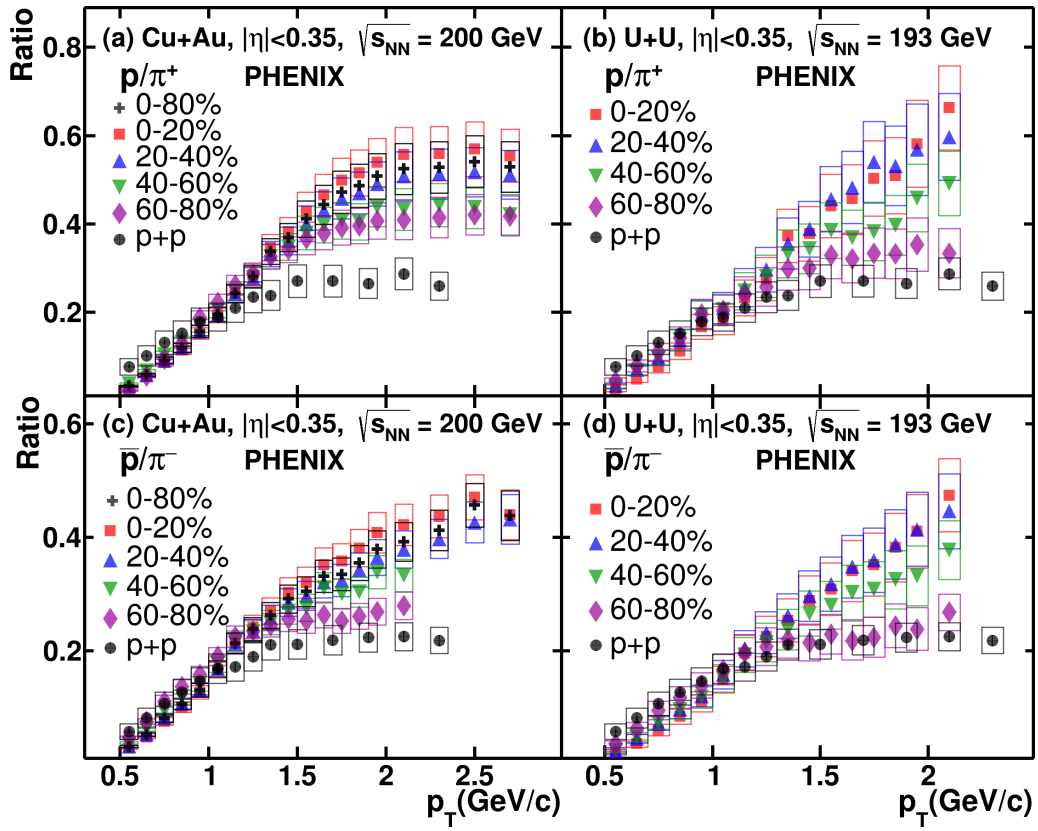

FIG. 9. The ratios of p/π^+ and $\bar{p}/\pi^-$ as a function of p_T measured in different centralities of Cu + Au and U + U collisions. Data points measured in $p+p$ collisions [43] are shown for comparison.

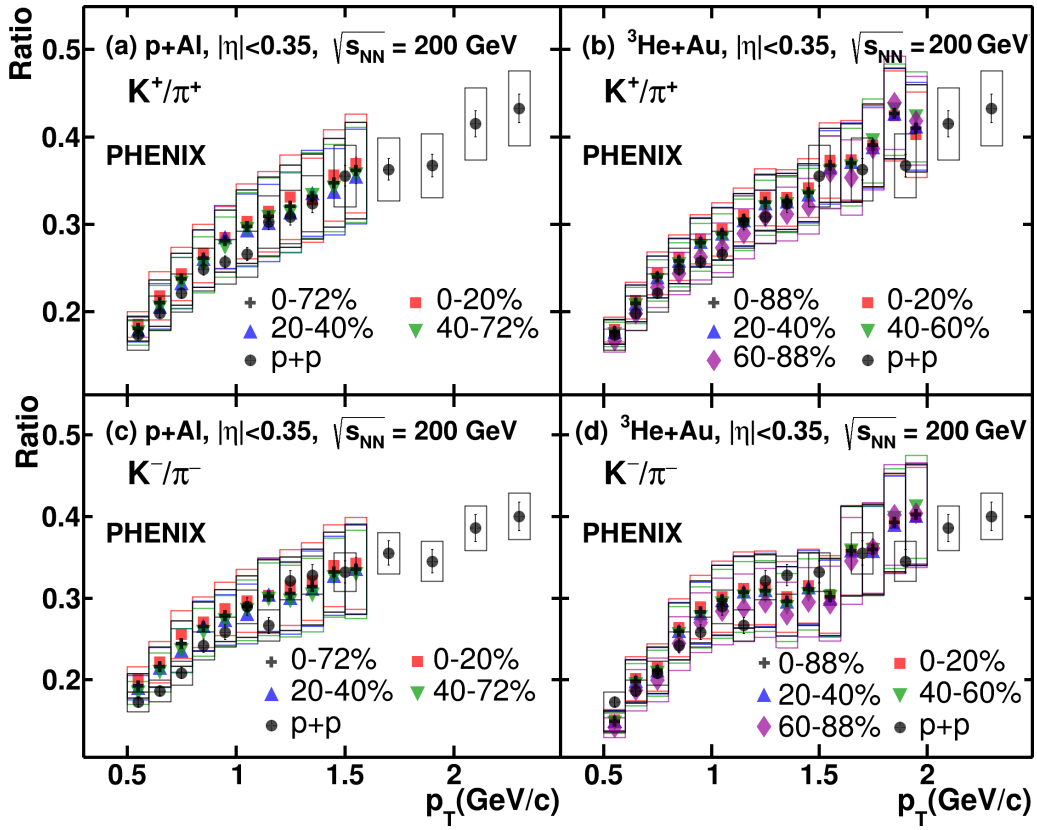

FIG. 10. The ratios of K^+/π^+ and K^-/π^- as a function of p_T measured in different centralities of $p+$Al and ^{3}He$+$Au collisions. Data points measured in $p+p$ collisions [43] are shown for comparison.

In heavy ion collisions (Cu + Au and U + U) the p/π ratios exhibit strong centrality dependence, but in small ^{3}He$+$Au collisions the centrality dependence is much more modest due to the much smaller range of $\langle N_{\rm part}\rangle$ values. Within uncertainties, the p/π values measured in each centrality of $p+$Al collisions are consistent with those measured in $p+p$ collisions. The values of the K/π ratios show a modest centrality dependence, which is insignificant within systematic uncertainties. The observed behavior of p/π and K/π ratios can be qualitatively described through hadronization by recombination [23,24].

Comparison of identified charged-hadron nuclear-modification factors shows that in $d+$Au, ^{3}He$+$Au, Cu + Au, Au + Au, and U + U collision systems the R_{AB} values are consistent at the same number of participant nucleons $\langle N_{\rm part}\rangle$. This indicates that identified charged-hadron production does not depend on the geometry and collision species, but rather is determined by system size alone (as indicated by $\langle N_{\rm part}\rangle$ values). Further, it is found that (i) the slope of $R_{AB}(p_T)$ in $p+$Al collisions is flatter than in ^{3}He$+$Au and $d+$Au collisions at the same $\langle N_{\rm part}\rangle$ values and (ii) proton R_{AB} values in $p+$Al collisions are equal to unity in the range of $1.0 < p_T < 2.5$ GeV/c, while proton R_{AB} values measured in ^{3}He$+$Au and $d+$Au collisions are larger than unity. Despite the observed absence of proton enhancement in $p+$Al collisions, there were evidences of QGP formation found by the PHENIX experiment in studies of J/ψ, $\psi(2S)$, and charged-hadron production at backward rapidity [48]. The observed differences in identified charged hadron production in $p+$Al and $d/^3$He$+$Au collisions may be caused by the size of the system created in $p+$Al collisions being too small to observe the expected increase in proton production.

ACKNOWLEDGMENTS

We thank the staff of the Collider-Accelerator and Physics Departments at Brookhaven National Laboratory and the staff of the other PHENIX participating institutions for their vital contributions. We acknowledge support from the Office of Nuclear Physics in the Office of Science of the U.S. Department of Energy, the National Science Foundation, Abilene Christian University Research Council, Research Foundation of SUNY, and Dean of the College of Arts and Sciences of Vanderbilt University (USA); Ministry of Education, Culture, Sports, Science, and Technology and the Japan Society for the Promotion of Science (Japan); Natural Science Foundation of China (People's Republic of China); Croatian Science Foundation and Ministry of Science and Education (Croatia); Ministry of Education, Youth, and Sports (Czech Republic); Centre National de la Recherche Scientifique, Commissariat à l'Énergie Atomique, and Institut National de Physique Nucléaire et de Physique des Particules (France); J. Bolyai Research Scholarship, EFOP, HUN-REN ATOMKI, NKFIH, and OTKA (Hungary); Department of Atomic Energy and Department of Science and Technology

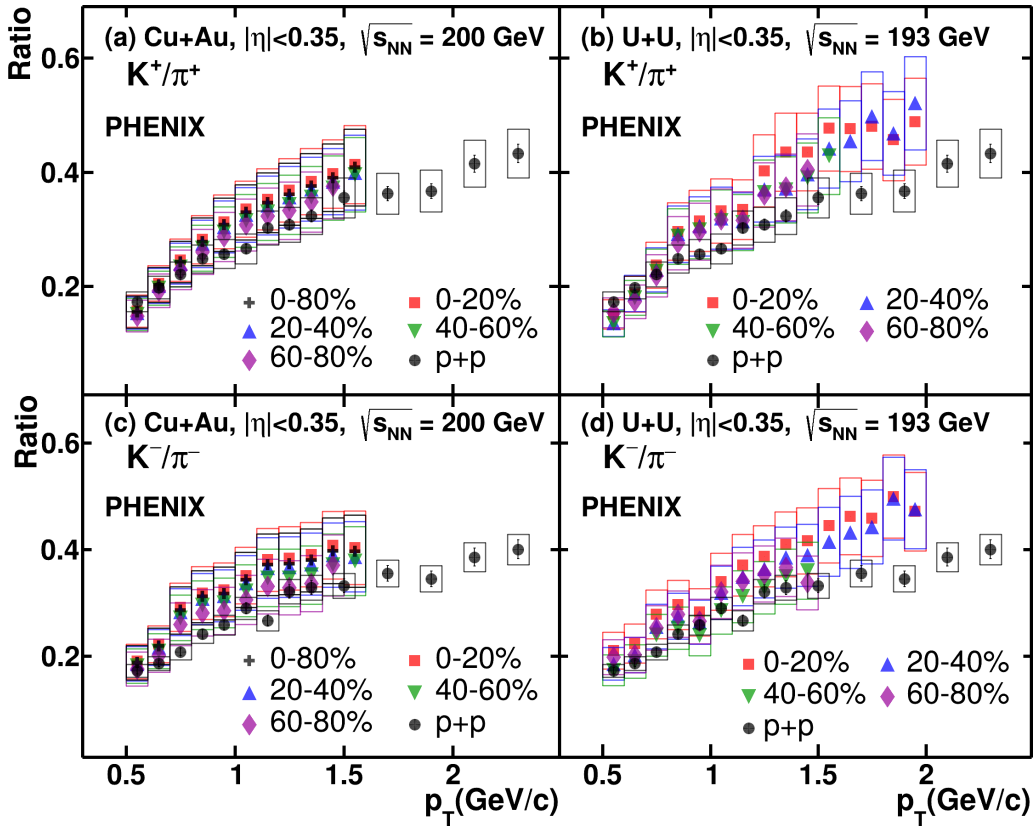

FIG. 11. The ratios of K^+/π^+ and K^-/π^- as a function of p_T measured in different centralities of Cu + Au and U + U collisions. Data points measured in $p + p$ collisions [43] are shown for comparison.

(India); Israel Science Foundation (Israel); Basic Science Research and SRC(CENuM) Programs through NRF funded by the Ministry of Education and the Ministry of Science and ICT (Korea); Ministry of Education and Science, Russian Academy of Sciences, Federal Agency of Atomic Energy (Russia); Knut and Alice Wallenberg Foundation (Sweden);

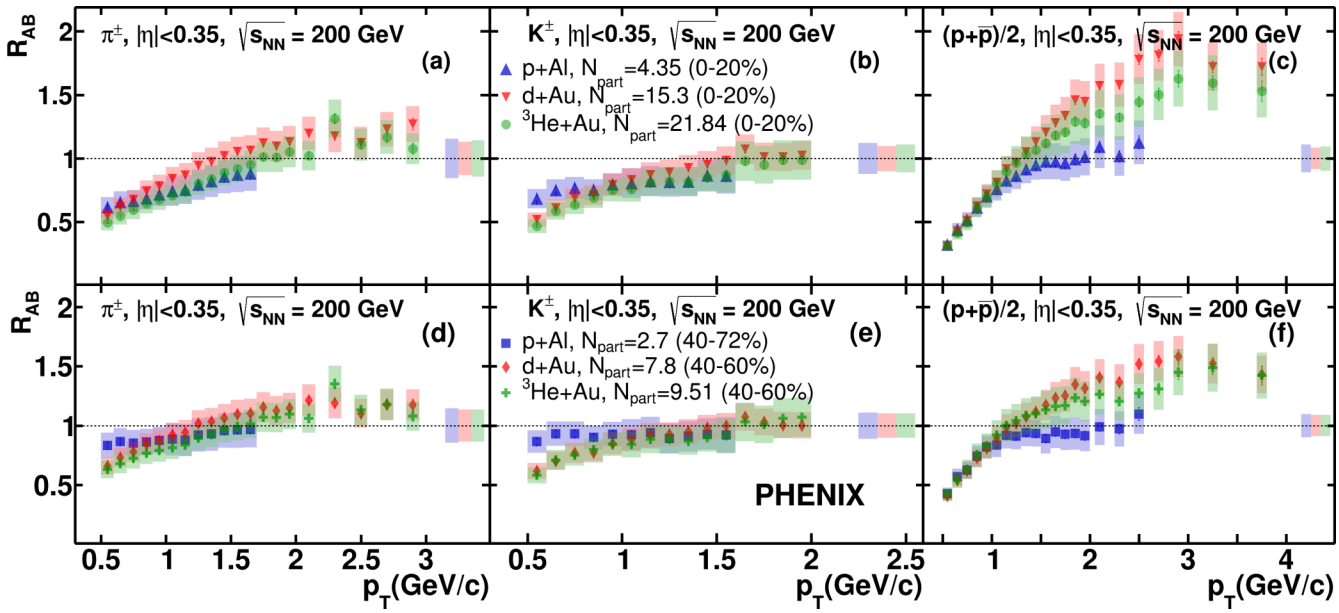

FIG. 12. Identified charged-hadron nuclear-modification factors as a function of p_T measured in central and peripheral $p + \mathrm{Al}$, $d + \mathrm{Au}$, and $^3\mathrm{He}$ +Au collisions. The dashed lines are drawn as a visual aid at the value of $R_{AB} = 1$ indicating absence of nuclear modification.

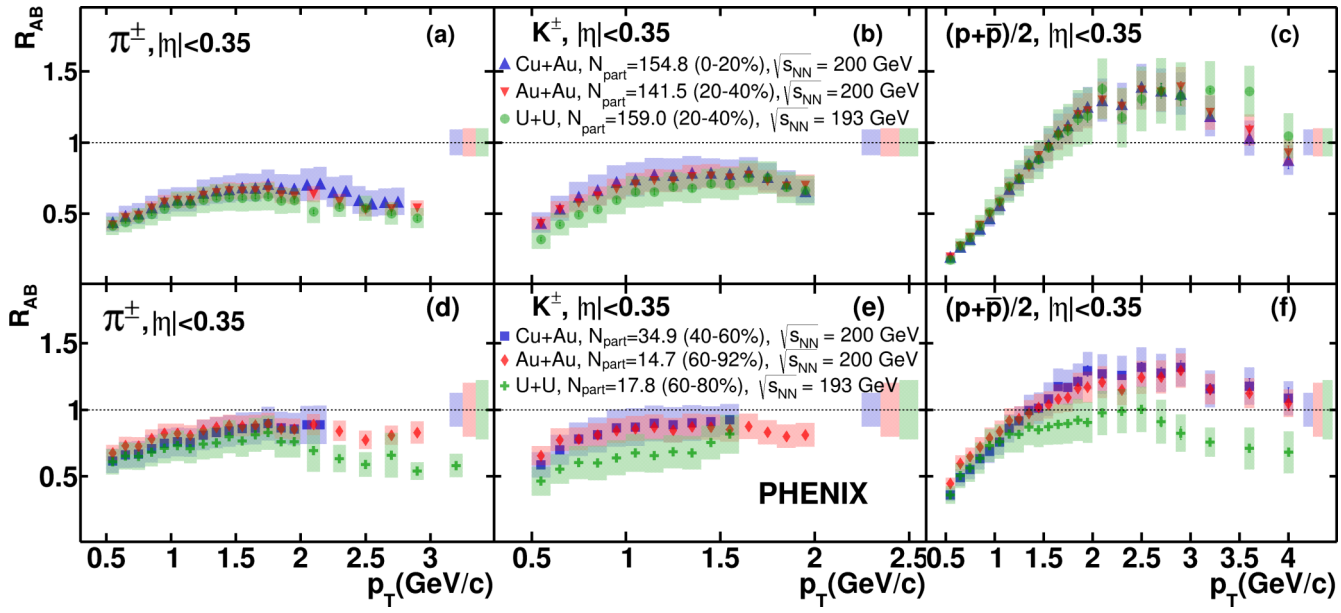

FIG. 13. Identified charged-hadron nuclear-modification factors as a function of p_T measured in central and peripheral Cu + Au, Au + Au, and U + U collisions. The dashed lines are drawn as a visual aid at the value of $R_{AB} = 1$ indicating absence of nuclear modification.

University of Zambia, the Government of the Republic of Zambia (Zambia); the U.S. Civilian Research and Development Foundation for the Independent States of the Former Soviet Union; the Hungarian American Enterprise Scholarship Fund; the U.S.-Hungarian Fulbright Foundation; and the U.S.-Israel Binational Science Foundation.

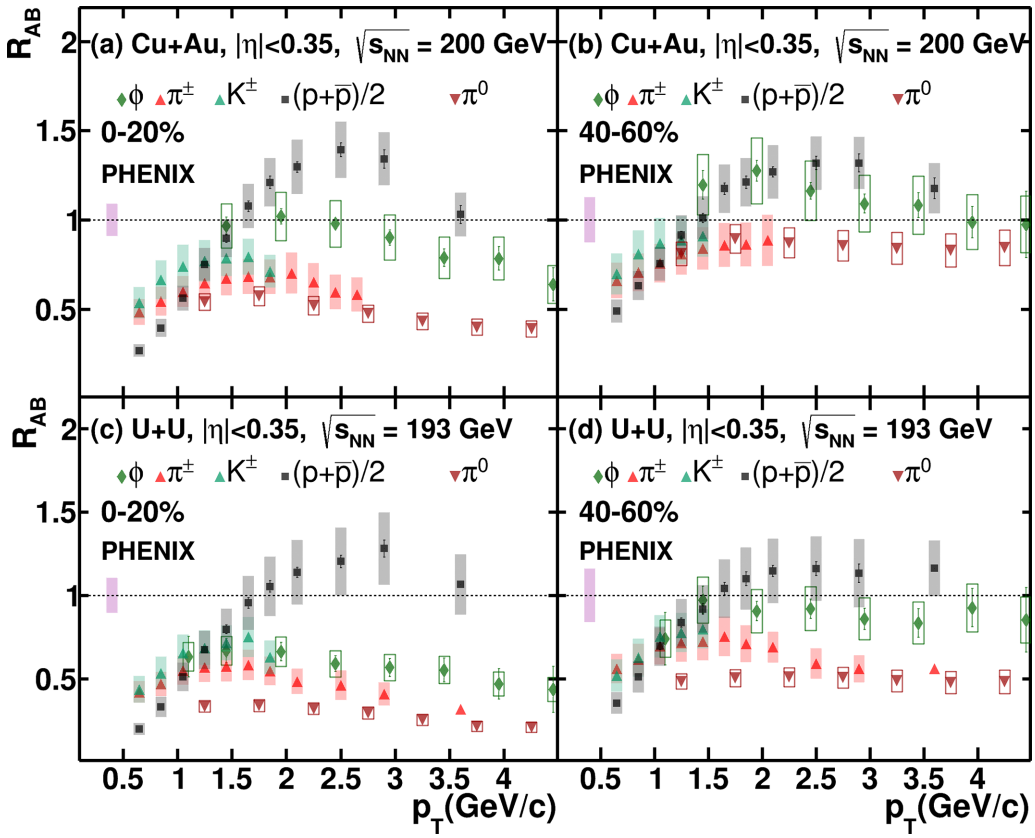

FIG. 14. Light hadron [ϕ [6], $\pi^{\pm}$, $K^{\pm}$, $(p + \bar{p})/2$, and π^0 [44,45]] R_{AB} values vs p_T measured in central and peripheral Cu + Au and U + U collisions. The dashed lines are drawn as a visual aid at the value of $R_{AB} = 1$ indicating absence of nuclear modification.

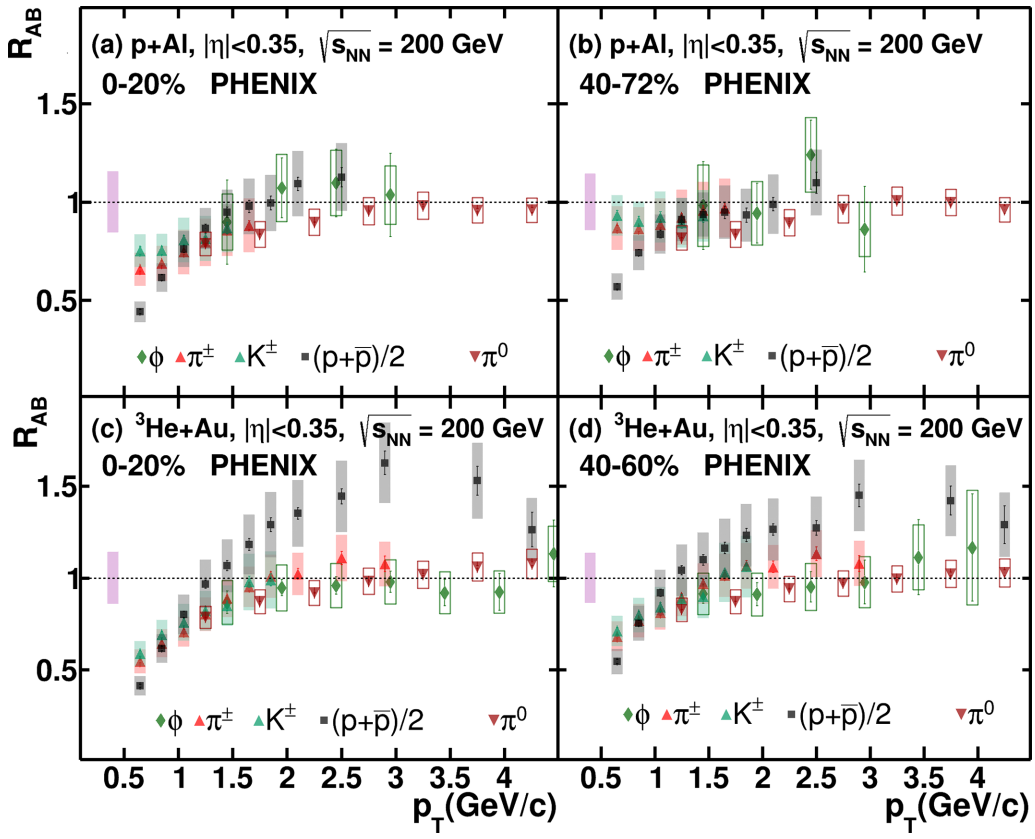

FIG. 15. Comparison of ϕ [26,46], $\pi^{\pm}$, $K^{\pm}$, $(p+\bar{p})/2$, and π^0 [47] R_{AB} values vs p_T measured in central and peripheral $p+\mathrm{Al}$ and $^3\mathrm{He}+\mathrm{Au}$ collisions. The dashed lines are drawn as a visual aid at the value of $R_{AB}=1$ indicating absence of nuclear modification.

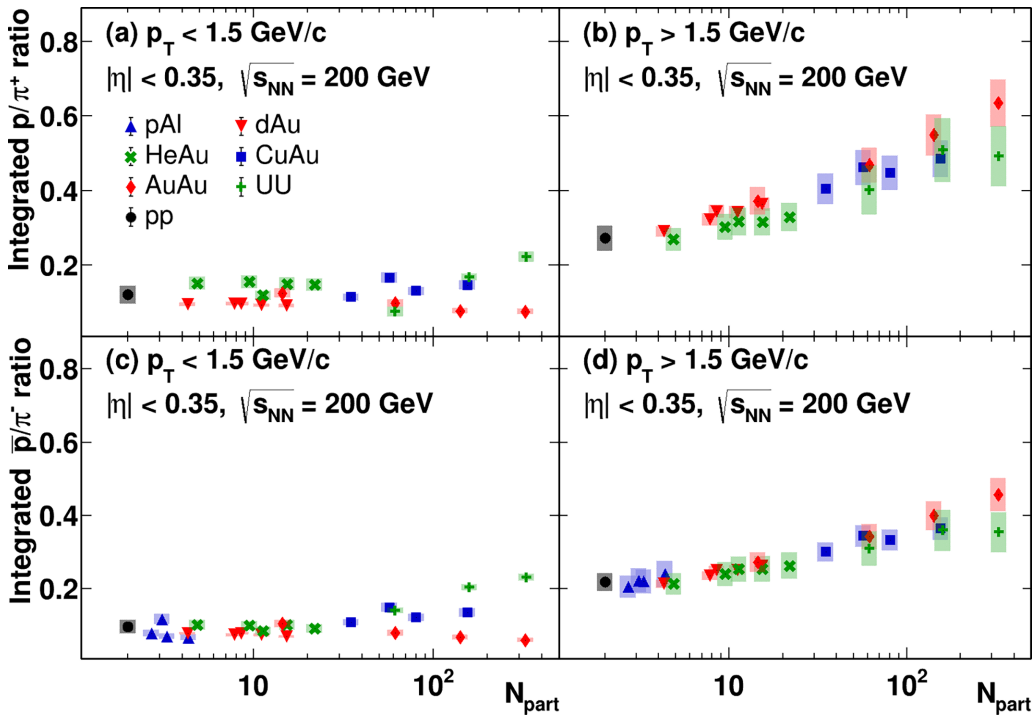

FIG. 16. The π^+, π^-, K^+, K^-, p, and $\bar{p}$ invariant p_T spectra measured in different centralities of $p+\mathrm{Al}$, $^3\mathrm{He}+\mathrm{Au}$, and $\mathrm{Cu}+\mathrm{Au}$ collisions at $\sqrt{s_{NN}}=200$ GeV and $\mathrm{U}+\mathrm{U}$ collisions at $\sqrt{s_{NN}}=193$ GeV. Invariant p_T spectra are multiplied by powers of 10 for clarity of presentation.

[1] K. Adcox *et al.* (PHENIX Collaboration), Formation of dense partonic matter in relativistic nucleus-nucleus collisions at RHIC: Experimental evaluation by the PHENIX Collaboration, Nucl. Phys. A **757**, 184 (2005).

[2] J. Adams *et al.* (STAR Collaboration), Experimental and theoretical challenges in the search for the quark gluon plasma: The STAR Collaboration's critical assessment of the evidence from RHIC collisions, Nucl. Phys. A **757**, 102 (2005).

[3] T. Niida and Y. Miake, Signatures of QGP at RHIC and the LHC, AAPPS Bull. **31**, 12 (2021).

[4] P. Koch, B. Muller, and J. Rafelski, Strangeness in relativistic heavy ion collisions, Phys. Rep. **142**, 167 (1986).

[5] P. Koch, B. Müller, and J. Rafelski, From strangeness enhancement to quark-gluon plasma discovery, Int. J. Mod. Phys. A **32**, 1730024 (2017).

[6] N. J. Abdulameer *et al.* (PHENIX Collaboration), Measurement of ϕ-meson production in Cu+Au collisions at $\sqrt{s_{NN}} = 200$ GeV and U+U collisions at $\sqrt{s_{NN}} = 193$ GeV, Phys. Rev. C **107**, 014907 (2023).

[7] F. Bellini (ALICE Collaboration), Strangeness in ALICE at the LHC, J. Phys.: Conf. Ser. **779**, 012007 (2017).

[8] S. Shi *et al.* (STAR collaboration), Strangeness in STAR experiment at RHIC, J. Phys.: Conf. Ser. **779**, 012008 (2017).

[9] D. Rohrich *et al.* (BRAHMS collaboration), Strangeness production at RHIC: recent results from BRAHMS, J. Phys. G **31**, S659 (2005).

[10] D. d'Enterria, 6.4 Jet quenching, in *Relativistic Heavy Ion Physics*, Landolt-Brnstein - Group I Elementary Particles, Nuclei and Atoms, Vol. 23, edited by R. Stock (Springer-Verlag, Berlin, Heidelberg, 2010), p. 471.

[11] S. Cao and X.-N. Wang, Jet quenching and medium response in high-energy heavy-ion collisions: A review, Rep. Prog. Phys. **84**, 024301 (2021).

[12] P. Lévai, G. Papp, G. Fai, M. Gyulassy, G. Barnafoldi, I. Vitev, and Y. Zhang, Discovery of jet quenching at RHIC and the opacity of the produced gluon plasma, Nucl. Phys. A **698**, 631 (2002).

[13] R. Reed *et al.* (ALICE Collaboration), Jet production in pp, pPb and PbPb collisions measured by ALICE, J. Phys.: Conf. Ser. **636**, 012010 (2015).

[14] S. S. Adler *et al.* (PHENIX Collaboration), Identified charged particle spectra and yields in Au+Au collisions at $\sqrt{s_{NN}} = 200$ GeV, Phys. Rev. C **69**, 034909 (2004).

[15] K. Adcox *et al.* (PHENIX Collaboration), Centrality dependence of π^+/π^-, K^+/K^-, p and anti-p production from $\sqrt{s_{NN}} = 130$ GeV Au+Au collisions at RHIC, Phys. Rev. Lett. **88**, 242301 (2002).

[16] J. Velkovska, p_T distributions of identified charged hadrons measured with the PHENIX experiment at RHIC, Nucl. Phys. A **698**, 507 (2002).

[17] A. Adare *et al.* (PHENIX Collaboration), Spectra and ratios of identified particles in Au+Au and d + Au collisions at $\sqrt{s_{NN}} = 200$ GeV, Phys. Rev. C **88**, 024906 (2013).

[18] B. B. Back *et al.* (PHOBOS Collaboration), Identified hadron transverse momentum spectra in Au+Au collisions at $\sqrt{s_{NN}} = 62.4$ GeV, Phys. Rev. C **75**, 024910 (2007).

[19] J. Adams *et al.* (STAR collaboration), Identified hadron spectra at large transverse momentum in p+p and d+Au collisions at $\sqrt{s_{NN}} = 200$ GeV, Phys. Lett. B **637**, 161 (2006).

[20] R. Fries, V. Greco, and P. Sorensen, Coalescence models for hadron formation from quark-gluon plasma, Annu. Rev. Nucl. Part. Sci. **58**, 177 (2008).

[21] L. Kumar (for the STAR collaboration), Identified hadron production from the RHIC beam energy scan, J. Phys. G **38**, 124145 (2011).

[22] K. Adcox *et al.* (PHENIX Collaboration), PHENIX detector overview, Nucl. Instrum. Methods Phys. Res., Sect. A **499**, 469 (2003).

[23] V. Greco, C. M. Ko, and P. Lévai, Parton coalescence and the antiproton/pion anomaly at RHIC, Phys. Rev. Lett. **90**, 202302 (2003).

[24] R. C. Hwa and C. B. Yang, Scaling behavior at high p_T and the p/π ratio, Phys. Rev. C **67**, 034902 (2003).

[25] C. O. Dorso, P. A. G. Molinelli, J. I. Nichols, and J. A. Lopez, Cold nuclear matter, arXiv:1211.5582.

[26] D. Pal (for the PHENIX Collaboration), ϕ meson production in d+Au collisions at $\sqrt{s_{NN}} = 200$ GeV, J. Phys. G **31**, S211 (2005).

[27] M. Krelina and J. Nemchik, Cronin effect at different energies: From RHIC to LHC, EPJ Web Conf. **66**, 04016 (2014).

[28] M. Shao *et al.* (STAR collaboration), Cronin effect at RHIC, AIP Conf. Proc. **828**, 49 (2006).

[29] E. Wang and X.-N. Wang, Jet tomography of hot and cold nuclear matter, Phys. Rev. Lett. **89**, 162301 (2002).

[30] K. Kovařík, A. Kusina, T. Ježo, D. B. Clark, C. Keppel, F. Lyonnet, J. G. Morfín, F. I. Olness, J. F. Owens, I. Schienbein, and J. Y. Yu, nCTEQ15: Global analysis of nuclear parton distributions with uncertainties in the CTEQ framework, Phys. Rev. D **93**, 085037 (2016).

[31] M. Abdallah *et al.*, Measurement of cold nuclear matter effects for inclusive J/ψ in $p+Au$ collisions at $\sqrt{s_{NN}} = 200$ GeV, Phys. Lett. B **825**, 136865 (2022).

[32] C. Aidala *et al.* (PHENIX Collaboration), Creation of quark-gluon plasma droplets with three distinct geometries, Nat. Phys. **15**, 214 (2019).

[33] K. Adcox *et al.* (PHENIX Collaboration), PHENIX central arm tracking detectors, Nucl. Instrum. Methods Phys. Res., Sect. A **499**, 489 (2003).

[34] L. Carlén *et al.*, A large-acceptance spectrometer for tracking in a high multiplicity environment, based on space point measurements and high resolution time-of-flight, Nucl. Instrum. Methods Phys. Res., Sect. A **431**, 123 (1999).

[35] M. Allen *et al.* (PHENIX Collaboration), PHENIX inner detectors, Nucl. Instrum. Methods Phys. Res., Sect. A **499**, 549 (2003).

[36] M. Aizawa *et al.* (PHENIX Collaboration), PHENIX central arm particle ID detectors, Nucl. Instrum. Methods Phys. Res., Sect. A **499**, 508 (2003).

[37] S. S. Adler *et al.* (PHENIX Collaboration), High p_T charged hadron suppression in Au + Au collisions at $\sqrt{s_{NN}} = 200$ GeV, Phys. Rev. C **69**, 034910 (2004).

[38] S. Adler *et al.* (PHENIX Collaboration), PHENIX on-line and off-line computing, Nucl. Instrum. Methods Phys. Res., Sect. A **499**, 593 (2003).

[39] R. Brun, F. Bruyant, F. Carminati, S. Giani, M. Maire, A. McPherson, G. Patrick, and L. Urban, GEANT detector description and simulation tool, Report No. CERN-W5013, CERNW-5013, W5013, W-5013 (1994), https://cds.cern.ch/record/1082634?ln=en.

[40] A. Adare *et al.*, Centrality categorization for $R_{p(d)+A}$ in high-energy collisions, Phys. Rev. C **90**, 034902 (2014).

[41] E. Schnedermann, J. Sollfrank, and U. Heinz, Thermal phenomenology of hadrons from 200A GeV S+S collisions, Phys. Rev. C **48**, 2462 (1993).

[42] V. Greco, C. M. Ko, and P. Lévai, Partonic coalescence in relativistic heavy ion collisions, Phys. Rev. C **68**, 034904 (2003).

[43] A. Adare *et al.* (PHENIX Collaboration), Identified charged hadron production in $p+p$ collisions at $\sqrt{s} = 200$ and 62.4 GeV, Phys. Rev. C **83**, 064903 (2011).

[44] C. Aidala *et al.* (PHENIX Collaboration), Production of π^0 and η mesons in Cu+Au collisions at $\sqrt{s_{NN}} = 200$ GeV, Phys. Rev. C **98**, 054903 (2018).

[45] U. Acharya *et al.* (PHENIX Collaboration), Production of π^0 and η mesons in U+U collisions at $\sqrt{s_{NN}} = 192$ GeV, Phys. Rev. C **102**, 064905 (2020).

[46] U. Acharya *et al.* (PHENIX Collaboration), Study of ϕ-meson production in $p+$Al, $p+$Au, $d+Au$, and ^{3}He +Au collisions at $\sqrt{s_{NN}} = 200$ GeV, Phys. Rev. C **106**, 014908 (2022).

[47] U. Acharya *et al.* (PHENIX Collaboration), Systematic study of nuclear effects in $p+$Al, $p+$Au, $d+$Au, and ^{3}He +Au collisions at $\sqrt{s_{NN}} = 200$ GeV using π^0 production, Phys. Rev. C **105**, 064902 (2022).

[48] U. Acharya *et al.* (PHENIX Collaboration), Measurement of $\psi(2S)$ nuclear modification at backward and forward rapidity in $p+p$, $p+$Al, and $p+$Au collisions at $\sqrt{s_{NN}} = 200$ GeV, Phys. Rev. C **105**, 064912 (2022).